3. A New Global Database of Mars Impact Craters to 1 km: 2. Global and Regional Properties and Their Implications to Gravity Scaling

Note: This paper is in preparation as: Robbins, S.J., and B.M. Hynek. "A New Global Database of Mars Impact Craters to 1 km: 2. Global and Regional Properties and Variations, and Their Implications to Surface Properties and Gravity Scaling." (in prep. for Icarus). Though it has not yet been submitted, it is cited in this thesis as "Robbins and Hynek, 2011c." Sections have been re-numbered and some reformatting has been done to fit the formatting of the rest of this dissertation. References have been combined with all others at the end of this dissertation. Acknowledgments have been combined with others at the beginning of this dissertation.

Abstract: We have generated a new, 378,540-entry, global crater database of Mars, statistically complete for craters with diameters $D \geq 1$ km. In its current release, this database contains detailed morphologic and morphometric data for craters $D \geq 5$ km and interior morphologies for craters $D \geq 3$ km (future releases will extend these to smaller diameters). We use this database first to reexamine previously observed distributions and patterns to show its fidelity and then to further explore global relationships. Distributions of central pit and summit pit craters are studied and we find the geographic distribution supports a volatile-dependent formation model. With detailed topographic data for the largest crater database to-date, we have analyzed crater depth-to-diameter ratios for simple and complex morphologies across various terrains and for the planet as a whole, and we investigated the simple-to-complex morphology transition. We find results similar to those in the published literature, but we find a substantial terrain dependence on the simple-to-complex transition which occurs at ~11-km-diameter craters at high latitudes. This suggests a model that requires melting of volatiles during high-latitude crater formation that fill the crater during the modification phase but will still support the simple morphology to larger diameters. Overall, this database is shown to be comparable to previous databases where there is overlap and to be useful in extending prior work into new regimes.

3.1. Introduction

Having a uniform database of objects and features from which to refer, draw on, and analyze forms the backbone of much research in most fields of science today. Astronomy is no exception with catalogs predating recorded history and the first relatively large one compiled by the Greek astronomer Hipparchus over 2100 years ago. The advent of the telescope and better views of the heavens accelerated this tradition all the way to the present day where many terabytes are relegated to storing these data. The planetary science community has its own niche, and a subsection within that is held by crater catalogs.

Crater catalogs or databases (the term is used interchangeably in this work) can inform a

variety of investigations of planetary processes, surface properties, physics, and geology. The utility and application of a crater catalog almost always goes beyond the original scope and applications of the person or group who generated it. Large, generalized databases are thus the most useful because they can be applied to diverse questions.

To this end, we have compiled the largest planetary crater database that exists today. This Martian crater catalog contains 378,540 craters with diameters $D \geq 1$ km. In a process thoroughly described in our companion paper (Robbins and Hynek, 2011b, this volume), we include many dozen morphologic and morphometric descriptors for each crater; in the current release, interior morphology are included for craters $D \geq 3$ km, and ejecta morphology and morphometry and crater degradation states are included for craters $D \geq 5$ km.

To both illustrate the fidelity and utility of this work, we have reexamined many previous general trends and properties of Martian impact craters from throughout the literature. On a basic level, we illustrate the global distribution of giant basins, hundred-kilometer-sized craters, intermediately sized craters, and few-kilometer craters and show they agree well with previous work (Section 3.2). We also examine the fresh crater population in the context of global circulation models in that section. We continue to crater and ejecta morphology in Section 3.3, exploring the distribution of crater central peaks, central pits, summit pits, intracrater dune fields, and both radial and cohesive layered ejecta. Section 3.4 addresses revision of Martian crater topographic properties with the new data; it shows that rim heights are $\sim 2\times$ smaller than are found on the Moon. Sections 3.5 and 3.6 present detailed recalculations of the depth-to-diameter function for simple and complex craters and the simple-to-complex morphology transition. This is done globally and by terrain that yielded disparate results discussed in Section 3.7.

3.2. Global Crater Distributions

The global crater distribution of Mars is generally well characterized in the literature, especially for larger (multi-kilometer) sized craters. Besides existing generalized crater databases (*e.g.*, Barlow, 1988; Stepinski *et al.*, 2009; Salamunićcar *et al.*, 2011), global mapping

efforts have identified large craters and used smaller craters to deduce stratigraphic relationships and ages (*e.g.*, Scott and Tanaka, 1986; Tanaka, 1986; Greeley and Guest, 1987; Tanaka *et al.*, 2011). In addition to global studies, regional or type studies have been completed, such as mapping craters on the poles (*e.g.*, Banks *et al.*, 2010), mapping fresh craters (*e.g.*, Boyce and Garbeil, 2007), identifying craters formed in the last few years (*e.g.*, Byrne *et al.*, 2009; Daubar, 2011) determining ages of major impact basins (Nimmo and Tanaka, 2005), and age-dating larger craters themselves (Werner, 2008). What has not been previously shown is the global distribution of small, kilometer-scale impact craters, and this work is the first such study because it is the first time such a catalog exists. This section begins with basin and large crater distributions to provide context while the remainder examines small and fresh crater locations.

3.2.1. Basins ($D \gtrsim 1000$ km)

There are seven broadly recognized basins on Mars with $D \gtrsim 1000$ km, and these are listed in Table **3** (Scott and Tanaka, 1986; Greeley and Guest, 1987; Nimmo and Tanaka, 2005). They are included in this discussion for completeness' sake and values should be treated as approximate. The basins Acidalia, Chryse, and Prometheii have less than 50% of their rim identifiable today. In cases of Acidalia, Chryse, Utopia, and Hellas, the rim that is visible is mostly vague with the rims of Acidalia and Hellas by far the least distinct. All of these basins are ancient, dating to the Noachian epoch of Mars' geologic history (Nimmo and Tanaka, 2005). Isidis, the best preserved, is the youngest with an estimated age ~3.9 Ga, while Argyre is also well preserved and has an estimated age ~4.0 Ga (Nimmo and Tanaka, 2005). Prometheii's northern rim is reasonably clean and preserved, but the bulk of the basin lies beneath Mars' south polar cap, limiting any study. The remaining four are estimated as $\gtrsim$4.1 Ga (Nimmo and Tanaka, 2005).

The explicit qualifier of "broadly recognized" in the proceeding paragraph is because many different researchers and groups have suggested other impact basins on the planet. One of the more recent and contentious is the proposition that the entire northern lowlands (the Borealis

Table 3: Large accepted basins on Mars with approximate latitude, longitude, and diameters. In this table, location has been rounded to the nearest degree and diameter to the nearest 100 km.

Name	Latitude	Longitude	Approx. Diameter
Acidalia	47° N	338° E	2300 km
Argyre	-48° N	316° E	800 km
Chryse	25° N	328° E	1700 km
Hellas	-38° N	075° E	2200 km
Isidis	13° N	088° E	1200 km
Prometheii	-85° N	091° E	1200 km
Utopia	40° N	080° E	3200 km

basin) is the result of a now-identified potential impact event (Andrews-Hanna *et al.*, 2008). This is disputed because others model that such a planet-altering impact would nearly destroy the planet (*e.g.*, McGill and Squyres, 1991), and endogenic processes may adequately explain the dichotomy (*e.g.*, Šrámek and Zhong, 2010 and references therein). Similarly, many other basins and large craters have been suggested on the planet in work done mainly by Frey (*e.g.*, Frey, 2006, 2008). For example, Frey (2008) suggests fully 20 basins on Mars with diameters $D >$ 1000 km. However, while these are perhaps more accurately referred to (as the author does) as "quasi-circular depressions," these features and similar smaller ones are not broadly recognized by the community as definitively of impact origin.

3.2.2. Large Craters (100 - ~500 km)

Three hundred one craters $100 \leq D \lesssim 500$ km are identified in this catalog and shown in Fig. **13**. Of the seven craters $D > 400$ km in this group, three are unnamed. The largest in this range is an unnamed crater southeast of and partially buried by Schiaparelli (-6° N, 13° E, $D \approx 510$ km). The remaining two unnamed craters are located at -18° N, 331° E (~470 km) and -37°N, 3° E (~430 km). The four named craters are Schiaparelli, Huygens, Cassini, and Antoniadi. The 301 craters in this group are not uniformly distributed across the planet, as is clear in Fig. **13**. The craters in this range reflect both the Martian crustal dichotomy and the major volcanic provinces in that there are fewer craters at higher northern latitudes and the Tharsis and Elysium regions are devoid of large craters.

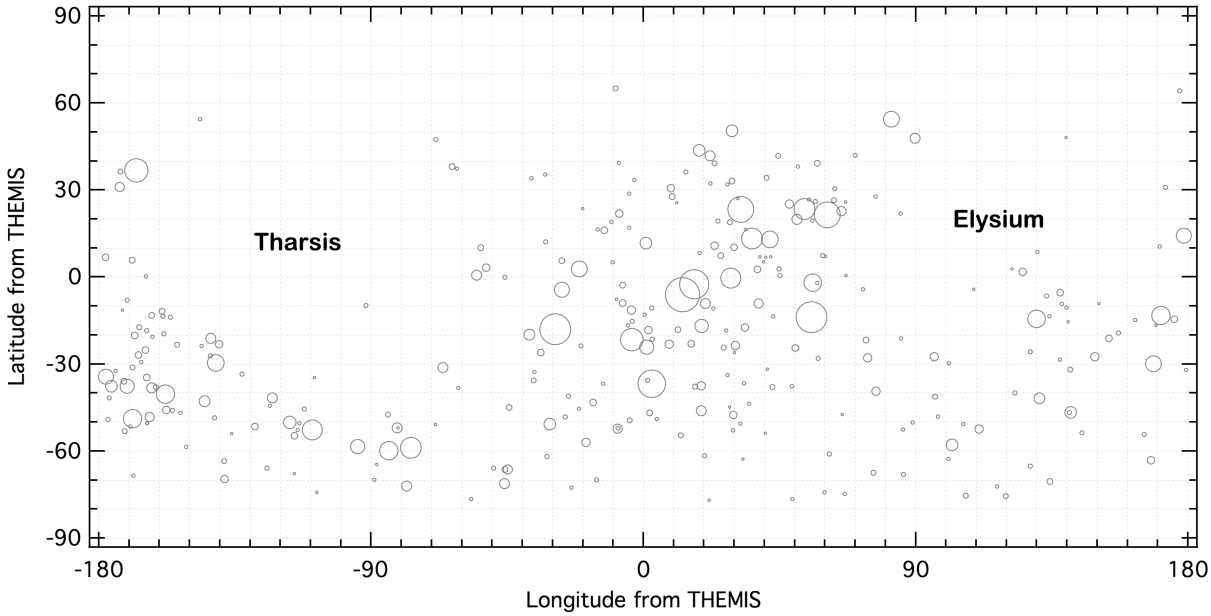

Figure 13: Locations and relative sizes of craters $100 \leq D \lesssim 500$ km on Mars. The large void around 20° N, -110° E is due to the Tharsis volcanic province, and the corresponding one ~100° E is due to the Elysium province.

3.2.3. Intermediate-Sized Craters (5-50 km)

This size range of craters has been well studied in the literature since imagery was first returned from spacecraft (*e.g.*, Chapman and Jones, 1977 and references therein; Tanaka, 1986 and references therein; Barlow 1988 and references therein). This range of craters, the locations of which are shown in Figure **14**, is mostly complex in morphology (save a very few simple craters up to ~15 km in diameter). Much of the early and current age-dating and stratigraphy work is done with this range of craters (see above references), and they inform studies of erosion rates, crustal strength, and scaling laws as will be discussed in subsequent sections. In a reflection of relative ages represented by crater densities in this size range, there are 560 craters per 10^6 km^2 on the averaged Noachian terrain, 207 on Hesperian, and only 98.4 on Amazonian. As a more detailed example, Chapman and Jones (1997) proposed there had been a large obliteration event early in Mars' history that buried craters $D \lesssim$ 20-30 km based on a relative lack of them. The same kind of deficit at this diameter range is observed in this database over much of the planet.

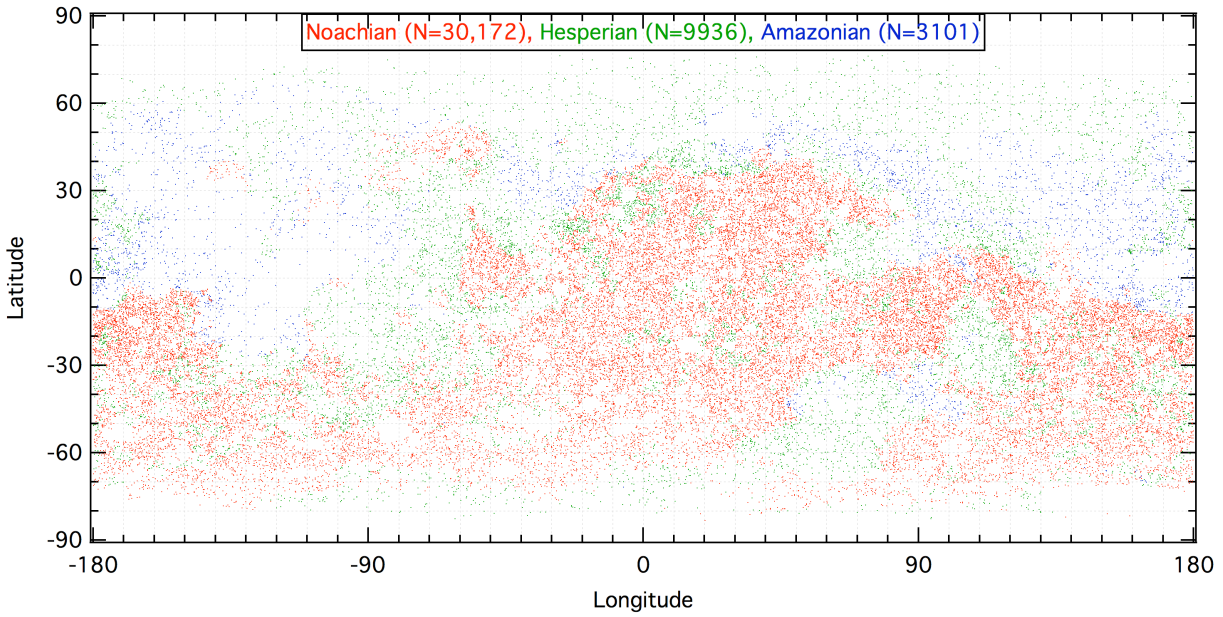

Figure 14: Map showing the distribution of all $5 < D \leq 50$ km Martian craters as a function of terrain age. Red dots represent craters on Noachian terrain, green are Hesperian, and blue are Amazonian. Terrain ages are from the Mars geologic maps (Scott and Tanaka, 1986; Greeley and Guest, 1987).

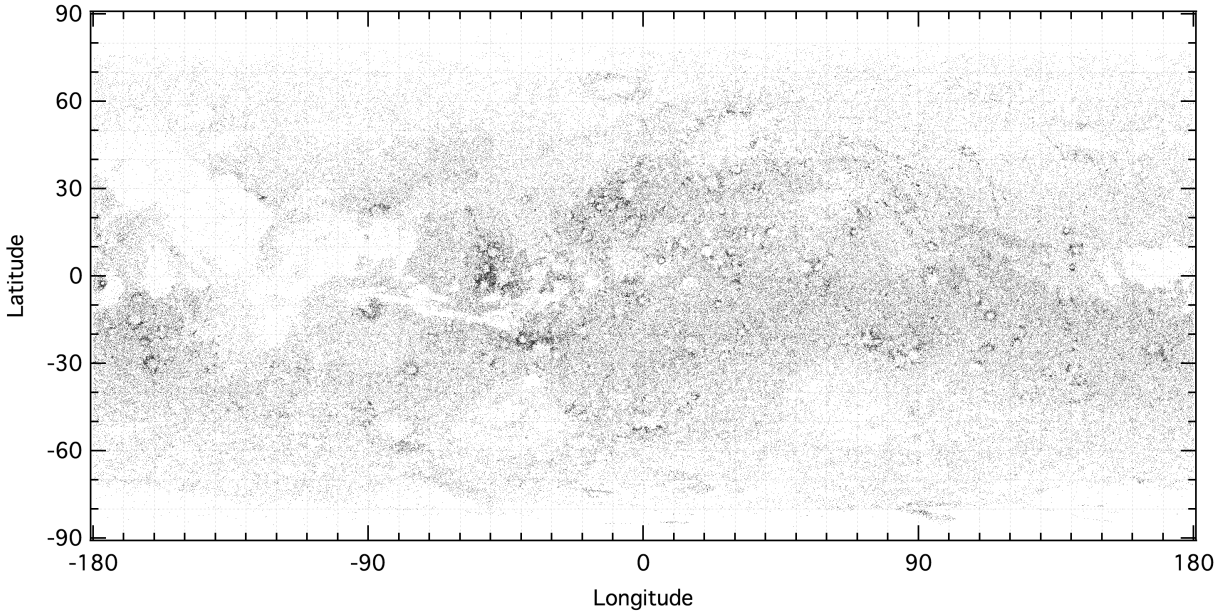

Figure 15: Locations of all $1 \leq D < 3$ km craters on Mars included in this database. This includes secondary craters; future releases of the database will have these separately marked.

3.2.4. Small Craters (1-3 km)

The small, $1 \leq D < 3$ km crater distribution on Mars is illustrated in Fig. **15**. The distribution of small craters can be used as a proxy for estimating relative regional ages - similar

to the larger size range discussed above - where more craters indicate an older surface and fewer craters indicate a younger surface. Readily visible as young surfaces due to their relative paucity of craters are the major basis Argyre and Hellas, the Olympus Mons volcano and three Tharsis Montes, Cerberus Planitia, Valles Marineris, and both polar caps. More locally, there is clear contamination from secondary crater fields closely surrounding individual large primary craters such as Lomonosov (65.3°N, -9.3°E) and Oudemans (-9.8°N, -91.8°E) (see Robbins and Hynek, 2011d (Section 4.2) for discussion of these fields). In addition, arcs of craters through Isidis are visible, emanating from Lyot crater (50.8°N, 29.3°E), and these are interpreted as secondary crater clusters from that large impact (Robbins and Hynek, 2011a (Section 4.1)).

3.2.5. Fresh Craters

Crater degradation/modification states were classified on a four-point scale. This was determined from analyzing each crater rim for sharpness and relief (1-4 pts), ejecta preservation (1-3 pts), floor infilling (1-4 pts), and relative depth/Diameter ratio (1-4 pts, determined based on latitude region; see Section 3.5). Points were added and then scaled to a final 1-4 class where 1 was the most modified and 4 was a pristine or nearly pristine crater. See the companion paper, Robbins and Hynek (2011b) for more detailed discussion of this classification (Section 2.4.4). These data are included in this release for all craters $D \geq 5$ km.

On an airless and geologically dead body, the distribution of fresh craters is nominally uniform over the surface since it should be of a uniform older age. On a body with an atmosphere and more recent geologic activity, such as Mars, the fresh crater distribution is instead a likely indicator of volcanic and aeolian erosion/modification efficiency across the planet (*e.g.*, Greeley *et al.*, 1992; Grant and Schultz, 1993) and periglacial processes on small craters near the poles. Fig. **16** shows the global distribution of $D \geq 5$ km fresh craters, and Fig. **17** shows the percentage of fresh $5 \leq D \leq 50$ km craters relative to all craters in that range. At a basic level, these show that weathering across the planet is far from uniform. Fresh craters are concentrated towards the equatorial regions and mid- to high-northern latitudes (between ~100-

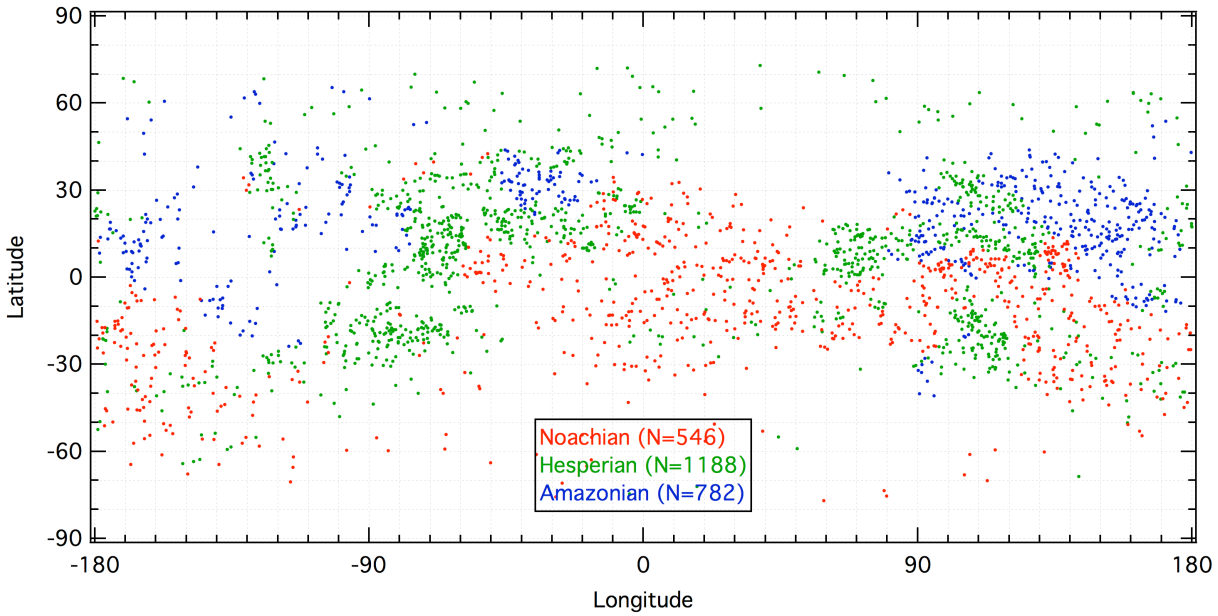

Figure 16: Scatter plot showing the distribution of all fresh $D \geq 5$ km fresh craters. Fresh craters are generally concentrated close to the equator but show a larger latitude range centered at ~200°E. Red dots represent craters on Noachian terrain, green are Hesperian, and blue are Amazonian. Terrain ages are from the Mars geologic maps (Scott and Tanaka, 1986; Greeley and Guest, 1987).

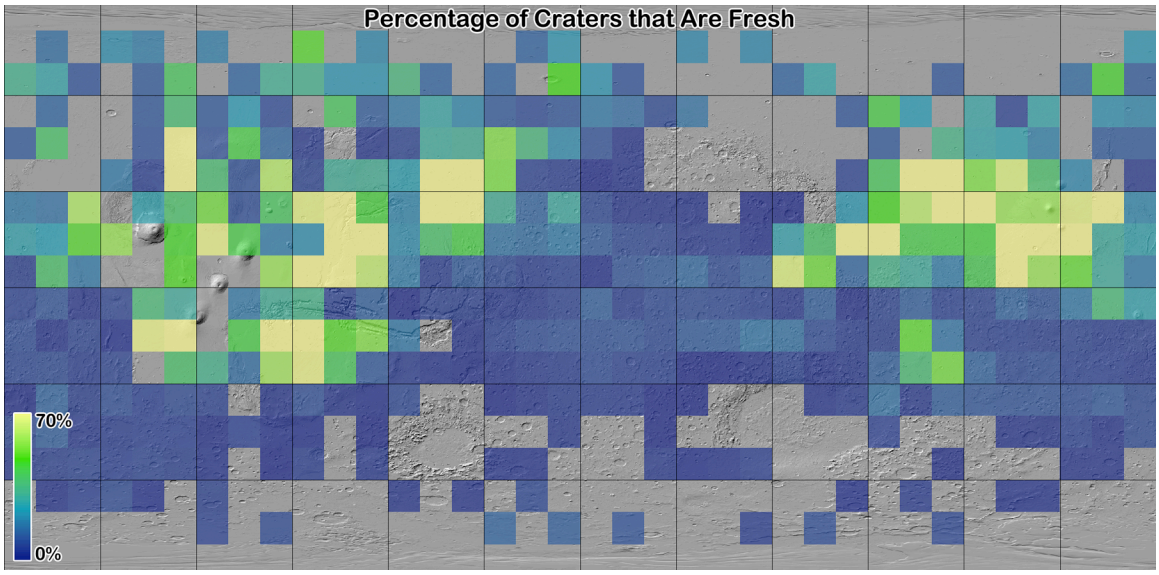

Figure 17: Area density plot showing the relative fraction of craters in 10°x10° bins that are fresh versus the population of all 5-50-km-diameter craters. Gaps are where there were not enough craters for an analysis or there were 0% fresh craters. Graticules are 30°.

300°E). They are also more frequently found on younger terrain, as expected: Spatially, there are 14.5 craters per 10^6 km^2 of Noachian terrain, 24.8 for Hesperian, and 17.3 for Amazonian.

The greatest fractional concentrations of fresh craters (Fig. **17**) are centered around the major volcanic provinces Tharsis, Elysium, and Syrtis Major, and the three basins Chryse, Isidis, and Utopia. A smaller concentration is also located between the two volcanoes Tyrrhena and Hadriaca Paterae. One can conclude from this that fresh craters are at least $2\times$ more populous on volcanic terrain than other surfaces. There is a general abundance above the average in the mid- to high-northern latitudes, as well, that likely reflects their relative youth.

In looking at atmospheric effects, Greeley *et al*. (1993) ran Mars global circulation models (GCMs) of Mars' atmosphere to examine predicted versus identified dust deposition. They found aeolian activity is high in the southern subtropics (~15-30°S), northern plains, fretted terrain, and surrounding the Tharsis and Arabia Terra regions. They expected low aeolian activity in Tharsis, Arabia Terra, and Elysium. Overall, the fresh crater distribution found in this database does not match that predicted by Greeley *et al*. (1993).

Better computers, topography models, and numerical techniques have advanced GCMs over the past few several years. The recent work by Haberle *et al*. (2003) compares more favorably with the crater results. They predict higher winds around Elysium, Tharsis, north and west of Tharsis, and south of Elysium around ~30-60°S. Except the last region, this is in general agreement with the fresh crater distribution from Fig. **17**.

Positive correlation with recent GCMs supports the hypothesis that fresh craters track well with atmospheric circulation. They also indicate that older models such as by Greeley *et al*. (1993) are inaccurate. As newer models are developed, further correlation experiments should be done. This does not mean that terrain type may not play a role. As indicated above, fresh craters favor Hesperian-aged terrain by number density and volcanic and basin terrain by type. However, these are likely well correlated themselves with the GCMs which must take into account topography, so decoupling these effects may not be practical nor possible.

3.3. Crater Morphologies Across Mars

Crater interior morphologies are included in this release for craters $D \geq 3$ km and ejecta morphologies are included for $D \geq 5$ km. The interior morphologic indicators include basic morphologic type (simple or complex) if it could be determined and indicators for central peaks, central pits, and summit pits. Morphology descriptors of wall features such as terraces and floor features such as tectonics, channels, dunes, and other floor deposits are also noted. Ejecta morphologies and morphometries are detailed for Martian cohesive layered ejecta blankets. The general distributions and properties of crater morphologies are described in this section and compared with previous works.

3.3.1. Distribution of Central Peaks, Pits, and Summit Pits

A classic feature of a fresh complex crater is a central peak, produced by rebound during the crater formation process. Central peak craters number 3049 in this database. They represent a steady global average of ~6.3% of all craters $D \geq 15$ km, yet they comprise a disproportionate number of fresh craters (>90% of fresh craters $D \geq 15$ km contain central peaks). This likely indicates that many craters classified as "CpxFF" (complex, flat-floored) or "CpxUnc" (complex, unclassifiable) were originally central-peak craters but the peak has since been buried or eroded. This interpretation is buoyed by Fig. **18** (the fraction of craters $5 \leq D \leq 50$ km with central peaks) which clearly shows that central peak craters are generally present in a relatively even fraction throughout most of the planet. There is a noticeable deficit in a band of the southern highlands arcing from Argyre basin up to the equator at the meridian and back down through Hellas. Interestingly, this does not correlate well with Fig. **17**, the fraction of fresh craters by area. The fraction of central peaks is mildly enhanced in Arabia Terra and in the southern highlands south of ~60°S and between East longitudes ~-90° to ~+90°. These imply the prevalence of central peaks is not completely a function of basic crater scaling laws and aeolian erosional processes.

A feature of some central peak craters on Mars is a pit in the middle of the peak, a classification of "summit pit." Martian craters as well as those on Jupiter's moons Ganymede and Europa will also sometimes display central pits; these pits are also occasionally observed in

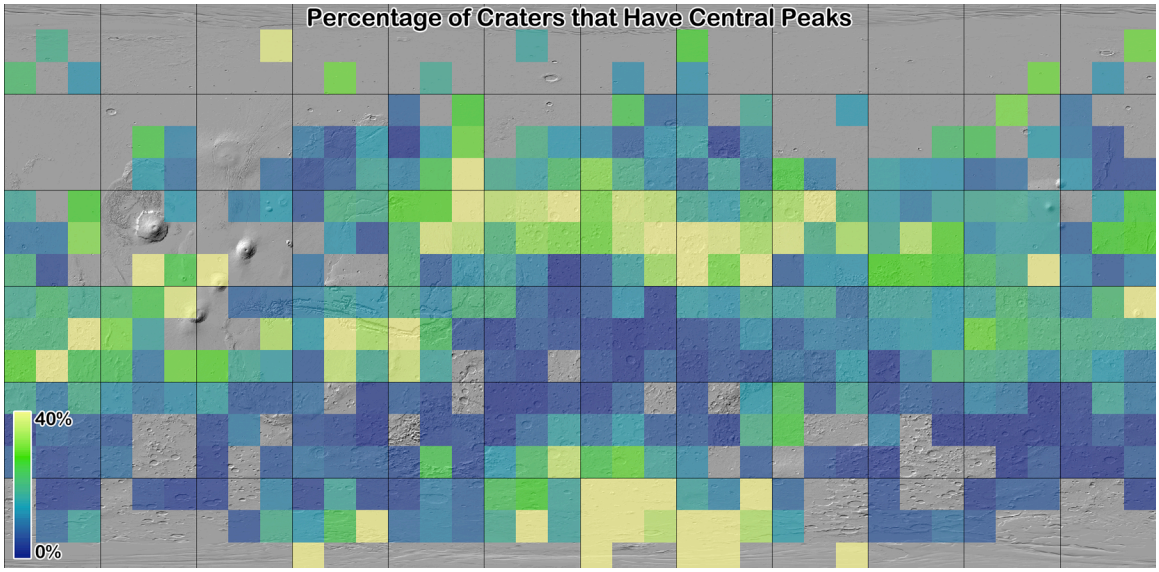

Figure 18: The fraction of craters $5 \leq D \leq 50$ km in 10°x10° bins that have central peaks. Underlying image is MOLA shaded relief. Gaps are where there were no craters, graticules are 30°x30°.

simple craters – unlike central peaks and, by extension, summit pits. Explanations for the genesis of these pits on crater floors or peaks are varied and include (1) vaporization of volatiles within the target during crater formation which releases gas near the center of the forming cavity (Wood *et al*., 1978; Senft and Stewart, 2008), (2) collapse of a central peak (Passey and Shoemaker, 1982), (3) excavation into layered target materials (Greeley *et al*., 1982), and/or (4) a melt-drainage model whereby liquid produced near to and during the impact forms a transient lake in the crater center that subsequently drains into the subsurface, leaving behind a central pit (Croft, 1981; Bray *et al*., 2006; Alzate and Barlow, 2011). The fraction of craters with summit pits (672 craters in all) are shown in Fig. **19**, and the fraction with central pits (1811 total) are shown in Fig. **20**.

It is difficult to draw many conclusions from the distribution of summit pit craters because of the small numbers involved, though they do generally agree with findings by Barlow (2011): They are prevalent in Arabia Terra, southwest of Tharsis, and southwest of Elysium. They appear to correlate well with the distribution of central peaks. This would not be surprising if their genesis is of the collapse mechanism suggested by Passey and Shoemaker (1982). However, there is a noticeable enhancement in the distribution north of Tharsis, and this is not observed in the

central peak distribution. There is likely a cryosphere near the surface at higher northern latitudes (Boynton *et al*., 2006) that would indicate a volatile-dependent origin. How ever, the significance of this is questionable: In each bin at that latitude (60-70°N), the number of craters with summit pits is 1. This lacks any statistical significance and so should not factor into any attempt to explain its formation other than as a footnote.

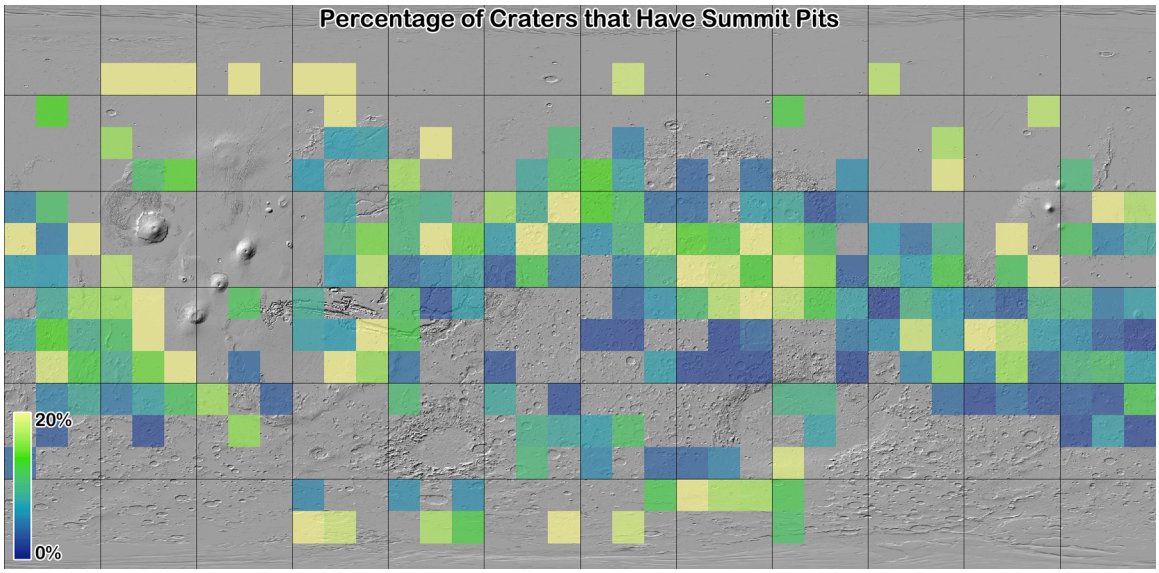

Figure 19: The fraction of craters $5 \leq D \leq 50$ km in 10°x10° bins that have summit pits. Underlying image is MOLA shaded relief. Gaps are where there were no craters, graticules are 30°x30°.

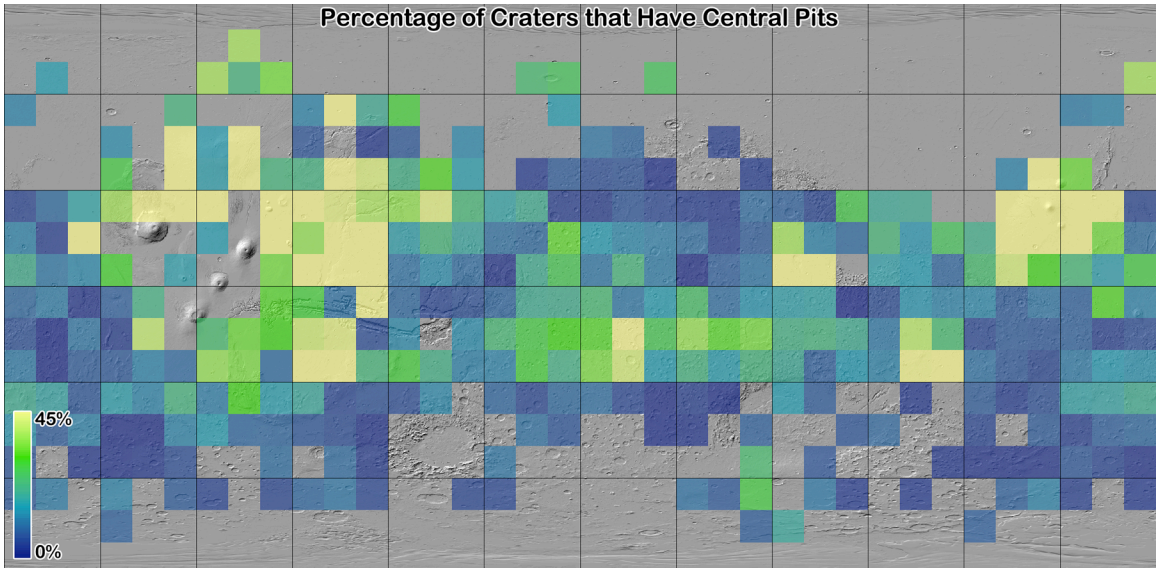

Figure 20: The fraction of craters $5 \leq D \leq 50$ km in 10°x10° bins that have central pits. Underlying image is MOLA shaded relief. Gaps are where there were no craters, graticules are 30°x30°.

Central pit craters are found to be enhanced relative to the global average around all volcanic centers, in general agreement with the findings by Barlow (2011): Tharsis, Elysium Syrtis Major, the Tyrrhena-Hadriaca corridor, and even southwest of Hells around Pitysua, Amphitrites, Peneus, and Malea Paterae. There is also an enhancement near the meridian and from about 0-30°S latitude. While these correlate with the fresh crater population, this is likely because the fresh craters correlate well with the volcanic terrain.

Subsurface ice near the equatorial Martian latitudes is not stable unless obliquities are >27°, and it is not stable in the Elysium region until obliquities are >30° (Mellon and Jakosky, 1995); if ice is present today near the equator, it is likely buried far below the surface (Clifford, 1993; Boynton *et al*., 2002). If the evacuation into subsurface liquid water reservoirs were the formation mechanism of central pits on Mars, though, one would expect significant concentration of central pit craters near the poles; this is not observed. Similarly, the central pit craters are generally among the fresh crater population (92% were a degradation state of 3 or 4), and they are missing in the high southern latitudes where central peaks were prevalent. Thus, they are likely not a collapse from a central peak. Of the four proposed mechanisms, the volatile vaporization and subsequent collapse and/or impact into layered material both fit the distribution observed, for volcanic terrain is generally enriched in volatiles, and it is often layered. The now-favored melt-drainage model in the literature (*e.g.*, Alzate and Barlow, 2011) appears to be less likely given the distribution, though it cannot be ruled out on this alone given the modeling that supports it (see Alzate and Barlow, 2011, and references therein). Further morphometric and mineralogy work may help constrain this, distinguish between the two, or show that one of the other mechanisms is more plausible.

3.3.2. In-Crater Dune Fields

Sand dunes on Mars are found both inside and outside of craters, and a comprehensive analysis culminated with the release of the Mars Global Digital Dune Database (MGD^3) by Hayward *et al.* (2007); this was supplemented by Hayward *et al*. (2008) and Fenton and

Hayward (2010). The original database was bound by ±65° latitude, omitting the poles, and it was constrained by the imagery at the time. Approximately 550 dune fields across the planet were included. The recent supplements expanded this coverage and identified a total of 1190 dune fields globally, both in and out of impact craters. In compiling this crater database, 777 craters $D \geq 3$ km were identified as containing dunes, and their locations are shown in Fig. **21**.

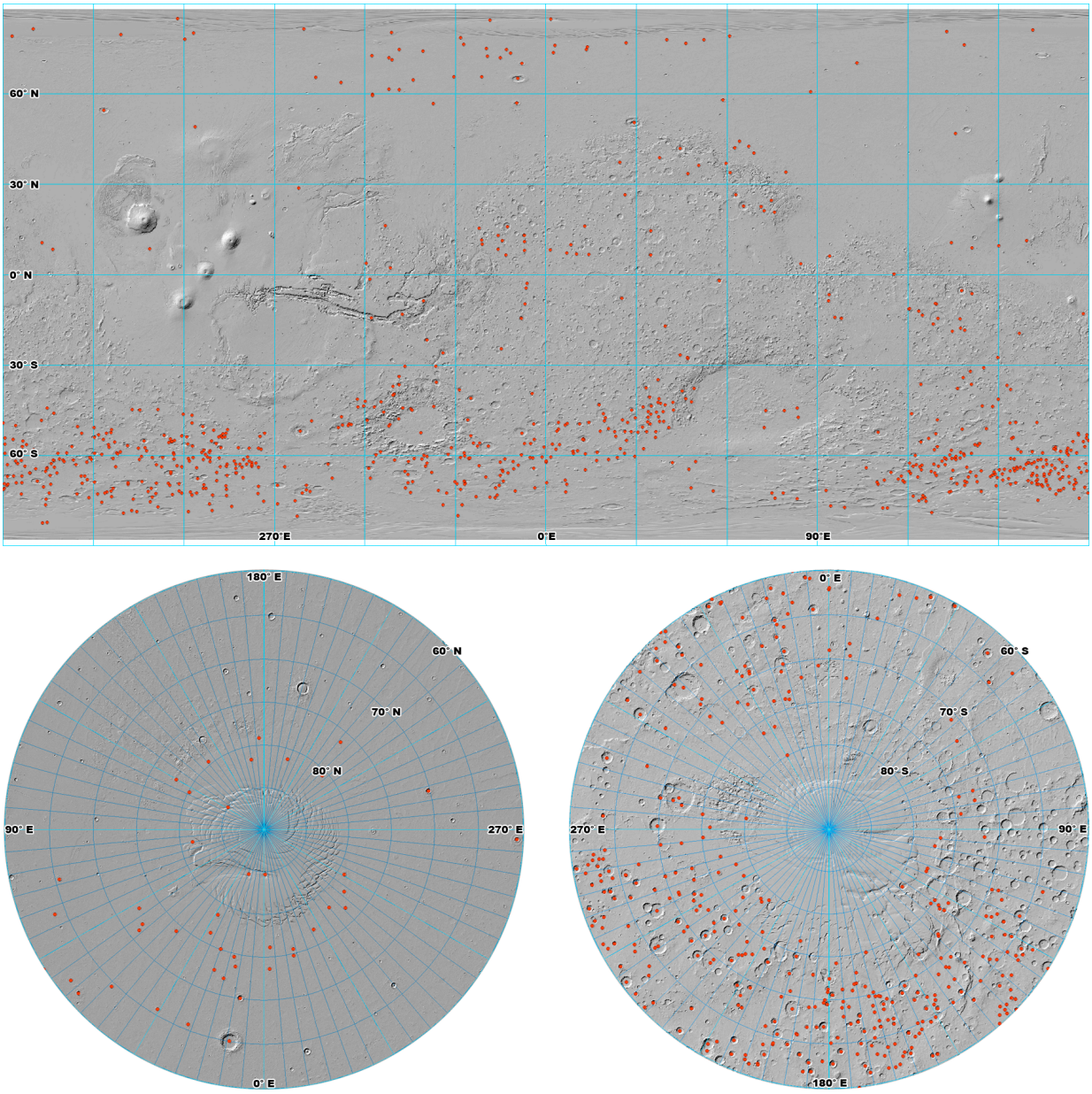

Figure 21: Locations of Martian dune fields in craters $D \geq 3$ km for Mercator (top) and north (bottom left) and south (bottom right) polar projections with MOLA-shaded and -colored relief underneath (Smith *et al.*, 2001).

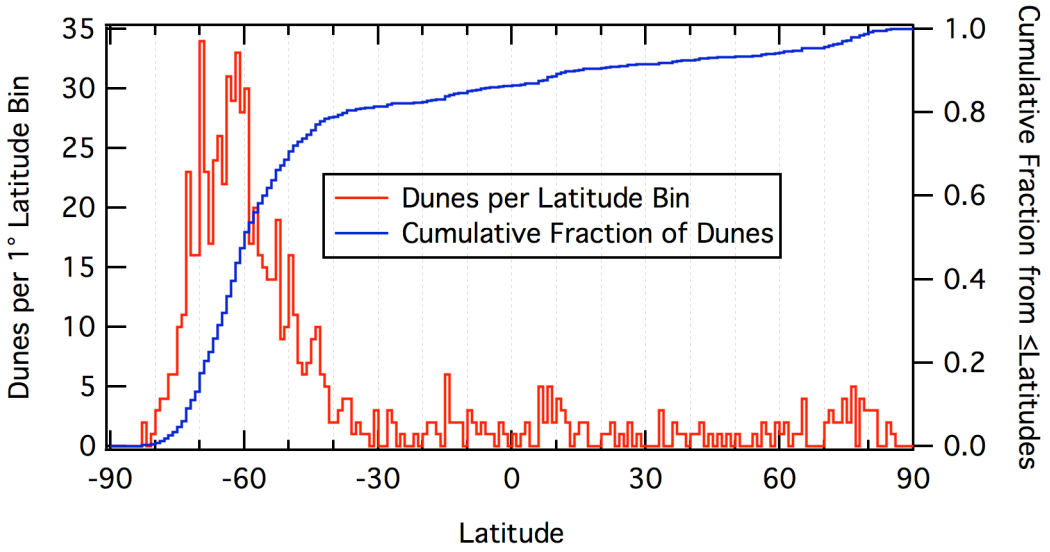

Figure 22: Latitudinal distribution of dunes within impact craters on Mars in 1°-wide bins. Red curve shows a basic histogram while blue is cumulative from the south to north pole and normalized to the total.

From Fig. **21**, a similar distribution as Hayward *et al.* (2007) is found with a large concentration west of Hellas, west of Argyre, and a large number between ~100° and 270°E longitude, south of ~50°S latitude. Numerous fields in the high southern latitudes between ~100° and 270°E agree well with Fenton and Hayward (2010). From Fig. **22**, the vast majority of these dunes (76%) are located south of -45°N, while 37% are located poleward of ±65°, indicating the original release of MGD^3 was missing at least 1/3 of in-crater fields. Northern dune fields are now present in MGD^3, but the relative abundance north of Acidalia were not observed, and there are some disparate results. For example, Hayward *et al*. (2008) identified 41 intracrater dune fields 65-90°N, while this database contains 36 (though this is within Poisson counting errors). Conversely, this database contains 30 craters 30-65°N latitude, while the MGD^3 contains eight. Future collaborations should better inform both datasets.

Preservationally, craters that contain dunes are generally more modified than average, as might be expected. 67% of them were marked with a "1" or "2" degradation state on the four-point scale, while 1% were a "4." This could be expected from comparison of the distribution with the overall fresh crater distribution in Section 3.2.5, as they are anticorrelated: Dunes are prevalent at southern latitudes where fresh craters are not, and the closest overlap in relative

densities is at roughly 60°S, 180°E. Following Section 3.2.5, this also correlates well with modern GCMs. However, there *are* otherwise fresh craters that do contain dunes - including several that are counted as "deep" among the deep crater population (see Section 3.5.2.3). This indicates that some large dune building on Mars likely took place in the recent past and may still be occurring today, in agreement with Fenton and Hayward (2010), who estimate that dune fields visible today formed an average of <1 Ma ago.

3.3.3. Ejecta Morphologies

Crater ejecta usually indicates crater youth, and on the Moon it is useful for geologic mapping and age relationships. On the Moon, craters display pure radial ejecta where the material has been ballistically emplaced during the excavation phase of crater formation as individual particles ejected during impacts. When probes returned the first images of Mars, however, a wholly new class of ejecta was observed. The terminology has varied significantly over the years (see companion paper, this volume (Section 2.4)), but the term "layered ejecta" is now part of the standardized nomenclature (Barlow *et al.*, 2000). This database contains morphologic indications for ejecta and morphometric data for the layered type that will be explored in brief in this section for craters $D \geq 5$ km.

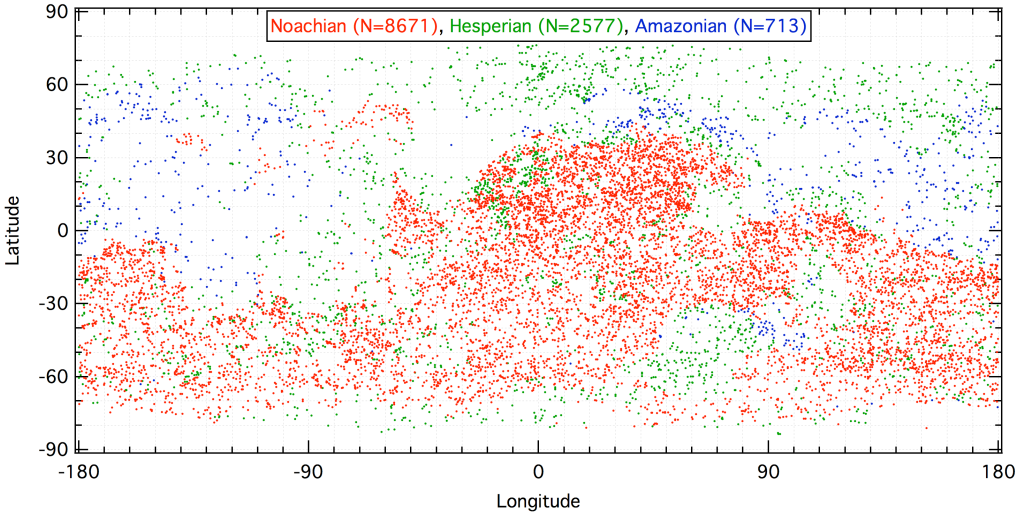

Figure 23: Scatter plot showing the distribution of all radial ejecta craters $D \geq 5$ km. Red dots represent craters on Noachian terrain, green are Hesperian, and blue are Amazonian. Terrain ages are from the Mars geologic maps (Scott and Tanaka, 1986; Greeley and Guest, 1987).

3.3.3.1. Radial Ejecta

Of the 46,482 craters $D \geq 5$ km in this database, radial ejecta is the sole ejecta type in 13,025 craters. They are shown as a function of terrain age in Fig. **23**. The spatial density on each terrain type is per 10^6 km^2: 161 Noachian, 54 Hesperian, and 23 Amazonian. It is clear from this that radial ejecta on Mars can still be visible around ancient craters, otherwise the distribution should be even. In fact, the relative densities are more disparate than those from the fresh crater population, as one would expect if this were the case.

3.3.3.2. Layered Ejecta

When Martian layered ejecta craters were first examined, it was thought they were part of a type evolution that started with multi-layered craters that erode to single-layer ejecta craters that finally erode to pedestal craters (McCauley, 1973; Arvidson *et al*., 1976). Woronow and Mutch (1980) and Mutch and Woronow (1980) were among the first to quantitatively examine the geometric properties of the ejecta of each and determine they are not evolutionarily related. Since then, two hypotheses emerged for a formation process of the layered ejecta. One holds that they are formed when an impactor hits a volatile-rich sub-surface, the impact energy melts or vaporizes the volatiles, and the ejecta acts like a fluid as a result (*e.g.*, Carr *et al.*, 1977). The other states that they form when the severity of the impact causes atmospheric vortexes and winds, but this generally requires a thicker Martian atmosphere to account for the extent of ejecta (*e.g.*, Schultz and Gault, 1979; Schultz, 1992). It is possible a combination of both models is at work on Mars (*e.g.*, Barlow, 2005; Komatsu *et al*., 2007).

Over the years, these forms of ejecta have only been observed on Venus, Mars, Ganymede, and Europa (*e.g.*, Barlow *et al*., 2000; Boyce *et al.*, 2010). The lack of atmosphere on Ganymede and Europa indicates that an atmosphere and hence the atmospheric vortex model is not required for the formation of these kinds of ejecta, but the intense surface heat on Venus would suggest that volatiles within the impact medium may also not be necessary in some formation situations. Determining the morphometric characteristics of each should help constrain these and discriminate between the two in different cases. Motivationally, if it can be

shown that morphometric analysis required volatiles for the ejecta to form, then high concentrations of these crater types could indicate where subsurface water may be for future human exploration. To this end, an introduction to the distributions and characteristics is presented here, and future work will focus on combining these with mineralogic, thermal inertia, and crater age dating of the ejecta blankets themselves to distinguish between the models.

Of the 46,482 craters $D \geq 5$ km in this database, a total of 12,621 craters are surrounded by layered ejecta blankets: 9265 are single-layered (SLE), 2571 are double (DLE), and 785 are multiple (three or more) (MLE). (See Robbins and Hynek (2011b) for a detailed description of all ejecta morphologic and morphometric properties in the database.) The Barlow Database (Barlow, 1988) over these diameters contains 3221, a factor of $\sim 4\times$ fewer. There is a size dependence observed on the number of layers. The largest SLE crater is a 111-km-diameter crater, the largest DLE is 78 km, and largest MLE is 83 km. These could be considered outliers, though, and insignificant in determining the onset of these features because all types start to increase dramatically on a size-frequency diagram at $D \sim 30-40$ km; they are statistically identical in frequency for $D \gtrsim 20$ km. For MLE, the peak in frequency is sharp and for craters

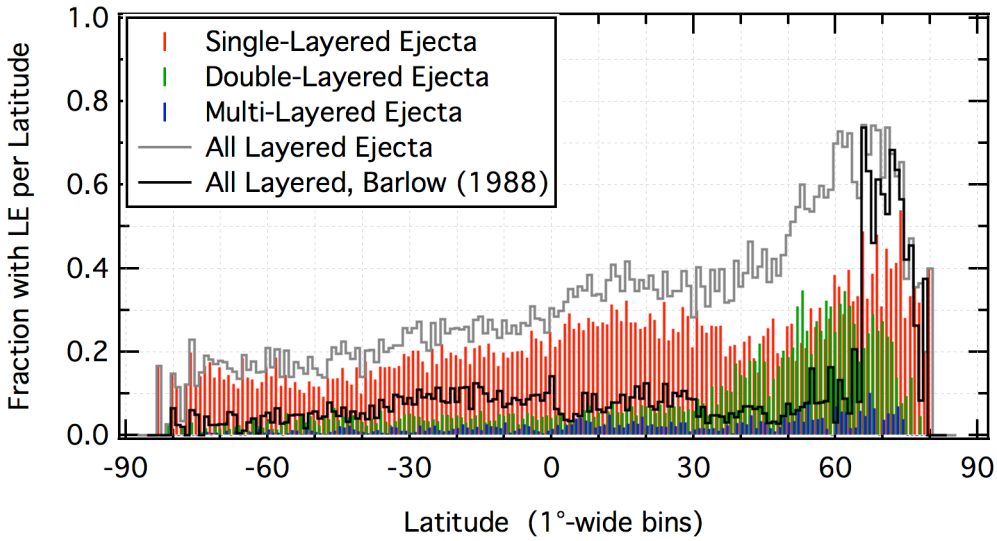

Figure 24: Distribution of layered ejecta craters, by type, per latitude bin. Red, green, and blue indicate SLE, DLE, and MLE distribution, respectively, while the grey line shows the sum of all three. For reference, the sum of all LE types from Barlow (1988) is shown as a black line.

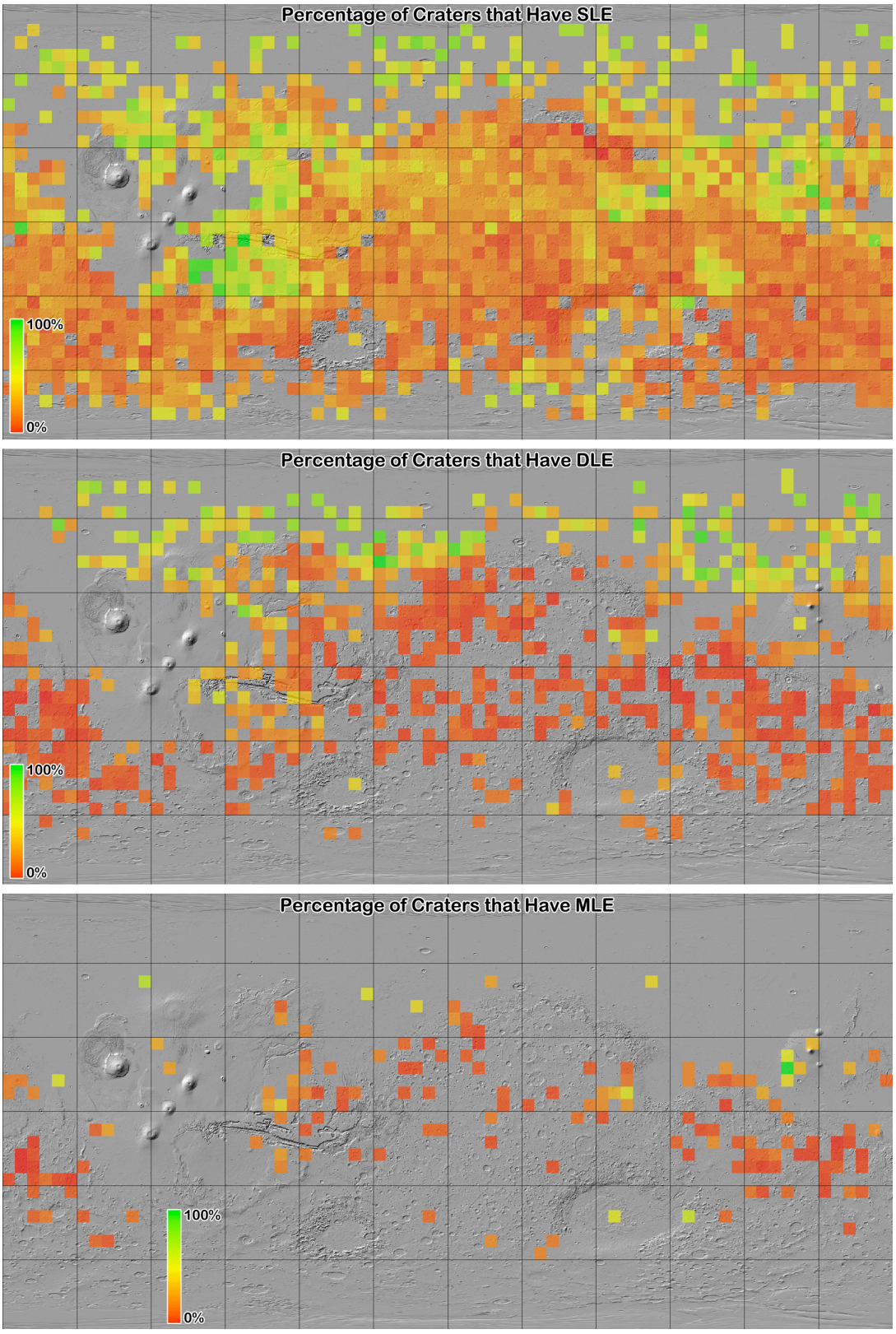

Figure 25: The fraction of craters $5 \leq D \leq 50$ km in 5°x5° bins that have layered ejecta blankets. Underlying image is MOLA shaded relief. Gaps are where there were ≤1 craters per bin, graticules are 30°x30°.

D = 17 km; it is rarer for a crater to display MLE blankets at smaller diameters. The peak for DLE is broader with a maximum at 12 km. No peak has been found for SLE craters, likely due to the size cut-off at 5 km for crater ejecta in this release of the catalog.

These craters are not distributed uniformly across the planet, a feature that has been known for many years (and characterized, for example, in Barlow, 1988). When examining the latitude-dependence, Fig. **24** clearly shows these craters are more numerous in the northern hemisphere and especially at high northern latitudes 50°-80° N. The enhancement around 10°N is likely due to volcanic terrain abundance at this latitude, discussed below. Barlow and Perez (2003) and Barlow (2005) found a relatively even distribution across the planet with a marked spike ~65-80° N. Another feature of the Barlow Database that this catalog reproduces well is the significant increase of DLE craters ~40-75°N (though Barlow and Perez (2003) found a tighter latitude range). Any mechanism to explain these features must include this as a hard constraint.

Expanding this distribution in longitude is shown in the three-panel Fig. **25** shows all SLE, DLE, and MLE craters as a fraction of all craters within a $5° \times 5°$ bin, similar to analyses in Barlow and Perez (2003) from Viking data. Clearly visible are several trends. First, SLE craters dominate all volcanic terrains (that have a significant number of craters on them). They also dominate in the high northern latitudes. DLE craters are similar though they clearly dominate at higher northern latitudes as indicated in Fig. **24**. In general, there was no longitude dependence upon the distribution of DLE craters, though there was a slight increase in the eastern Tharsis and lower Valles Marineris region. It is difficult to draw conclusions from the MLE distribution due to small numbers (even at coarser binning, global trends do not show). The most that can be confidently stated is that the MLE distribution does not disagree with the SLE distribution, and there is a significant enhancement around Elysium. These all agree with the general conclusions from Barlow and Perez (2003) with the main anomaly being the concentration of SLE craters to the southwest of Valles Marineris. This could be an artifact of the way the data are presented: In Fig. **24**, LE types are shown as a fraction of all craters, but in Barlow and Perez (2003), the data are discussed and displayed as a fraction of craters with ejecta.

Table 4: Average ejecta mobility values for select layered ejecta types.

	SLE	DLE Inner	DLE Outer
Global	1.4	1.4	2.5
<-40°N Latitude	1.6	1.5	2.5
±30° Latitude	1.2	1.2	1.8
>+40°N Latitude	2.0	1.5	3.2

A morphometric characteristic examined is ejecta mobility, the extent to which the ejecta travels relative to the crater radius. This database uses the average extent, following Barlow (2005). It reproduces her findings well, though the ejecta mobility is a little less in this work (see Table **4**). As a global average, ejecta mobility of SLE craters averages 1.4 versus 1.5 found by Barlow (2005). DLE inner layers are 1.4 (versus 1.5) and the outer is 2.5 (versus 3.2). The ejecta mobility maximums were found to be 8.8, 4.9, and 11.7, comparable if slightly larger than Barlow (2005). An additional feature identified in early work (Mouginis-Mark, 1979) is a latitude dependence with ejecta mobility where, near the poles, the average is up to 2.0 versus the equatorial average of 1.4. This catalog's data show a similar trend, while the change happens at ~±30-40°. Ranges poleward of ±40° were examined separately from an equatorial region ±30°, and values are reported in Table **4**. Polar crater layered ejecta is found to travel farther than equatorial, while that in the northern hemisphere travels farther than in the south. This is placed in context with other morphometric data from this catalog in the Discussion (Section 3.7).

3.4. Crater Shapes

Basic crater shapes have been measured for decades (*e.g.*, Pike, 1976), and this database provides the ability to verify and update these morphometric values on Mars. For this analysis, only fresh craters of degradation class 4 were used (1964 simple and 1413 complex). This section addresses crater rims and surface-to-floor scaling. Scaling of crater depth (rim-floor) as a function of diameter is described in Section 3.5. Both of these rely upon accurate rim height measurements, a value that is in question given the relatively coarse nature of MOLA gridded

data. The fidelity of measurements in this database was addressed in detail in Robbins and Hynek (2011b) (Section 2.3). To within the uncertainty quoted in the database in rim heights, it was found that the measurements from gridded data were accurate when compared with the MOLA point data.

The first feature often addressed is rim height above the surrounding surface. At a basic level, this scales with crater diameter, and Melosh (1989) reports generalized results based on lunar data that rim height is ~4% of the crater diameter. However, examination of the Martian craters in this database shows a well-defined Gaussian distribution of this relationship for simple craters 1.9±0.7% and 1.4±0.6% for complex craters. This rim height is $>2\times$ smaller than what is typically reported. A possible explanation is that this database uses the average elevation around the crater rim instead of the highest point, but that is unlikely to be able to account for this large of a difference. Similarly, Melosh (1989) quotes the surface-to-floor depth of simple craters to be ~20% the crater diameter, but the simple craters in this database have a relationship of 8.9±1.9%. This is again $>2\times$ smaller than what is typically reported. Complex craters are shallower with a surface-to-floor depth 6.2±1.9% the crater diameter.

When looking at a diameter-dependence for rim height, fresh craters were examined in the method detailed below for depth/Diameter relationships. For fresh simple craters, a power law $h = 0.011D^{1.300}$ was fit, and a relationship of $h = 0.025D^{0.820}$ was found for complex craters (where h is rim height and D is crater diameter). In contrast, Garvin *et al*. (2003) found $h = 0.04D^{0.31}$ for simple craters (significantly different) but $h = 0.02D^{0.84}$ for complex (statistically identical). Better topographic data for smaller-diameter craters should help determine which - if either - is accurate.

Another way to examine scaling is to measure rim height relative to the overall rim-to-floor crater depth. This is found to follow a Gaussian with a mean 16±6% for simple craters and 18±6% for complex craters. The similar if slight offset indicates that the uplift and overturn that results in rim formation scales well through these two crater morphologies.

3.5. Global depth/Diameter Relationships

The ratio of a crater's depth to its diameter is one of its most fundamental properties, but it is one that was not directly measurable for extraterrestrial craters until the last decade. Prior, crater depths were estimated through photoclinometry and shadow lengths, processes that rely on knowing sun angles and assuming a uniform surface albedo (*e.g.*, Chapman and Jones, 1977; Pike, 1976, 1977, 1980, 1988; Davis and Soderblom, 1984). With the inclusion of the MOLA instrument on *Mars Orbiter*, global laser altimetry data has allowed for the uniform measure of crater topographic properties provided in this database. These were measured from the MOLA gridded data (MEGDR) as described in Robbins and Hynek (2011b). Briefly, crater rims and floors were identified in MEGDR data and the average elevation of points along the rim and deepest sections of the floor were used to compute the rim-to-floor depth (used in this analysis). This was found to be accurate when compared with the MOLA point data (PEDR), though debate remains as to whether the MOLA data accurately reflect the true rim crest and true lowest points on crater floors for smaller craters (D < 7 km). Limited random sampling performed in Robbins and Hynek (2011b) suggests that the recorded values are accurate to within the uncertainties that were also recorded. Future work comparing these data with the *Mars Express*'s High-Resolution Stereo Camera (HRSC, Neukum and Jaumann (2004)) should clarify this, but at present the MOLA data are still used.

Previous work by Garvin *et al.* (2003) estimated a $d = 0.21D^{0.81}$ relationship for simple craters $D \leq 6$ km, and $d = 0.36D^{0.49}$ for complex craters $D > 6$ km. Boyce and Garbeil (2007) find a similar curve of $d = 0.315D^{0.52}$ for complex craters $D \geq 7$ km. While hesitant to quote a global average for reasons discussed below, this database yields a simple crater relationship of $d = 0.179D^{1.012}$ and a complex one of $d = 0.286D^{0.582}$; these are comparable to previous works, though there is some variation as one may anticipate. This section discusses the depth-to-diameter relationship for Martian craters from this crater database and goes into significant detail on regional variations in this function.

3.5.1. Regional depth/Diameter Relationships

Across the surface of a planetary body, one might expect the ratio of a crater's depth to diameter to be constant since it is a gravity-dominated feature (Melosh, 1989). But, while gravity dominates, terrain properties control this final ratio, as illustrated in this section. This affects any "global" depth/Diameter ratio (*d*/*D*) one may quote, as has been done throughout the literature for decades (*e.g.*, Pike, 1980; Garvin *et al.*, 2000, 2003; Boyce and Garbeil, 2007; Stepinski *et al.*, 2009). To illustrate this, craters were separated by simple and complex morphologies and then into different diameter ranges. Diameter ranges within each morphology were done because there is no set, quotable ratio for the *d*/*D* value for fresh simple or complex craters – even though it is quoted as 1:5 and 1:10-100, respectively (Pike, 1977; Melosh, 1989).

All craters were divided into six diameter ranges that each encompassed roughly a factor of 2× in size. Smaller ranges had small-number problems that limited the overall utility, while

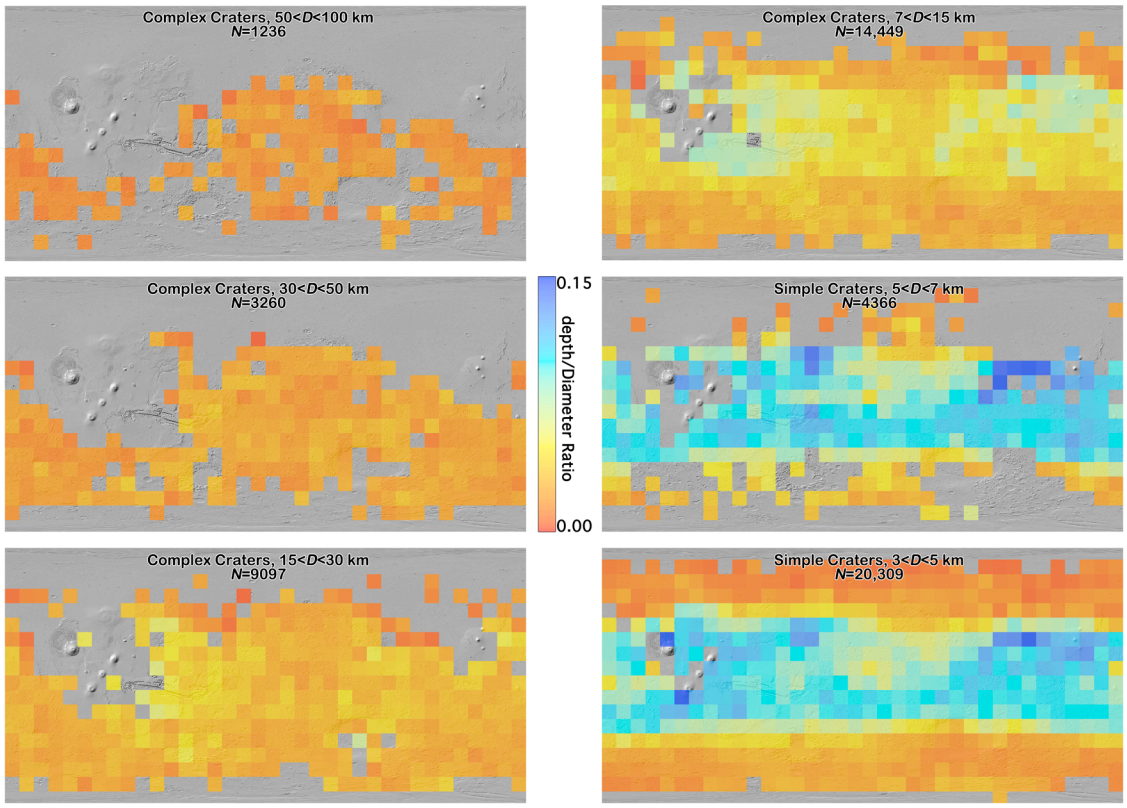

Figure 26: Six panels showing binned crater depth/Diameter ratios across Mars in 10°x10° bins; bins with $N < 5$ craters were removed. Four panels show complex craters and two are simple. All utilize the same color scale range of a depth/Diameter ratio of 0.00-0.15.

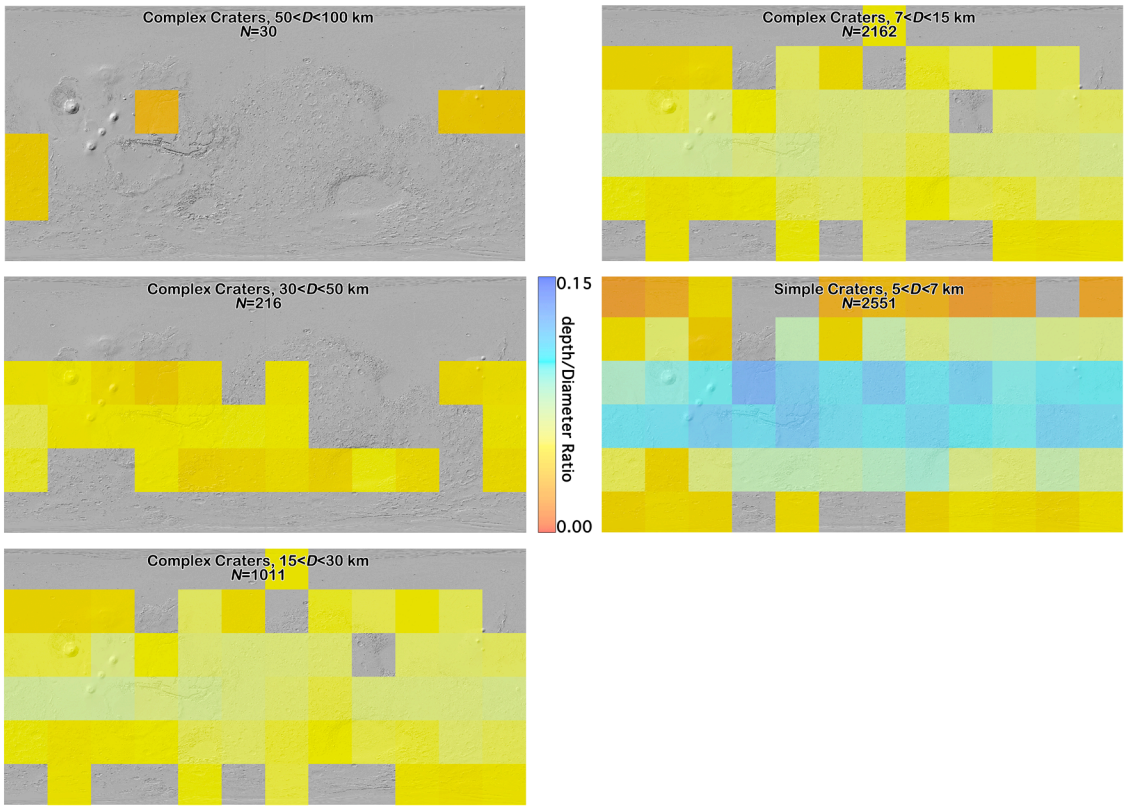

Figure 27: Five panels showing binned fresh (degradation states 3 and 4) crater depth/Diameter ratios across Mars in 30°x30° bins; bins with $N < 5$ craters were removed. Four panels show complex craters and one is simple (3-5 km-diameter crater degradation states were not calculated for this release of the crater database). All utilize the same color scale range of a depth/Diameter ratio of 0.00-0.15.

larger ranges muted the differences and hence analysis that could be done. Simple craters were separated into two ranges – 3-5 km (N=20,309) and 5-7 km (N=4366). Complex craters were separated into four: 7-15 km (N=14,449), 15-30 km (N=9097), 30-50 km (N=3260), and 50-100 km (N=1236). Craters were then binned into $10° \times 10°$ latitude/longitude bins and the mean d/D value was calculated; bins with <5 craters were removed. These are shown in Fig. **26**. A similar analysis was done for fresh craters only, illustrated in Fig. **27**, in $30° \times 30°$ bins and omitting the smallest diameter range. The results were comparable given the limitations, as discussed below.

Readily apparent from Fig. **26** is significant global variation. To first-order, craters $D \lesssim 20$ km poleward of ~±40° latitude are significantly shallower than their counterparts closer to the equator by as much as a factor of $2-3\times$. Second-order effects are that craters near the major volcanic complexes - Tharsis and Elysium - are deeper than the general average, and craters

within the Isidis, Utopia, and northern Chryse / southern Acidalia impact basins are the deepest on the planet, on average. Similar results were observed by Boyce *et al*. (2006), except they did not identify this effect in northern Chryse (this was not in their study area). In the equatorial range, the shallowest craters are within Arabia Terra, unique from the southern highlands. The patterns noted here disappear at larger crater diameters, or at least as far as can be determined based upon the smaller numbers. The last remnants of the pattern are in the 15-30 km range, showing the deeper craters around Tharsis and Elysium and shallower craters towards the north pole, but not the south. $D > 30$ km craters do not show this.

Analysis of the fresh crater population (degradation states 3 and 4) shown in Fig. **27** support the majority of these observations: Craters are shallower near the equator and deeper near the poles, and this effect persists up to the $D \leq 30$ km range. The more localized findings of deeper craters in the northern hemisphere basins is not found, though this is likely because of small number statistics; finer binning in the $5 \leq D \leq 7$ km simple crater range removes bins over those regions due to small numbers, so the effects are averaged out at the coarser binning shown. Deeper craters at small diameters are observed over the Tharsis region, though. The shallower craters observed in Arabia Terra are not observed at smaller diameters but are somewhat visible between 7 and 30 km, though the difference is slight. This overall agreement between Figs. **26** and **27** support the interpretation that Fig. **26** is generally indicative of the fresh crater population and the interpretations that follow.

The equatorial/polar dichotomy disappearing for $D > 30$ km craters is likely because larger craters formed with enough impact energy to be deep enough and no longer feel the effects of the local crust. Thus, their final shapes are nearly completely dictated by gravity scaling instead of being terrain-controlled. The pattern at smaller diameters of shallower craters towards the poles is likely explained by a near-surface cryosphere (Boynton *et al.*, 2002) that is weaker and cannot support a deep crater, relaxing to a shallower depth. This implies that the crust overlying the major impact basins Chryse, Isidis, and Utopia, is stronger than the average Martian surface today, supporting the deeper crater cavities. Expanding upon the argument from

Boyce *et al*. (2006), this shows that the local crust is stronger by at least a factor of 2× than most other surfaces on Mars. Mineralogical mapping in future work may help characterize the rock, as there are suggestions of regional olivine-rich units in southern Isidis that may play a role in this (Hamilton *et al*., 2003; Hoefen *et al*., 2003). Alternatively, the similarity with deeper craters on volcanic terrain and the gravitational load in the regions suggest these basins may be buried by volcanic material, and that could be stronger than the average Martian crust to ~1 km depths (*e.g.*, Searls and Phillips, 2007). A separate hypothesis - and it is possible that all three may be in play to various degrees - is that the terrain may be particularly fine-grained in some areas of these basins. Work suggests (*e.g.*, Soderblom *et al*., 1973, 1974; Schultz and Lutz, 1988) that fine-grained fill materials can produce anomalously deeper craters and that this material is found in at least some of these regions.

3.5.2. The d/D Relationship for Mars

3.5.2.1. Variation with Latitude and Terrain Type

As is readily apparent from Fig. **26**, except for craters $D \gtrsim 30$ km there is no uniform, global depth/Diameter ratio even for a small diameter range that can be quoted for the planet because of a significant shallowing near the poles. This must be taken into account when considering a relationship "for Mars" and when using it to determine different things at an automated level, such as its role in crater degradation state classification. Besides being important from a physical standpoint and understanding the near-surface crust, it is necessary to have an *a priori* estimate for how deep a crater likely was when it formed for purposes of estimating erosion and infilling. For example, if one were to use a global estimate for a $D = 5$ km simple crater ($d = 0.8$ km) and found it to be filled with lava with 0.2 km deep cavity remaining, then one would assume 0.6 km of burial. But, if this crater was poleward of ~40°, the actual d/D relationship yields a fresh crater depth of $d \approx 0.3$ km, so there is only 0.1 km of infill.

In the following sub-sections, craters were separated into seven different regions: First, a global average was done as has been worked on for several decades for comparison purposes.

Next, two latitude ranges were analyzed based upon Fig. **26** and Section 3.5.2.2 – poleward of ±40° and equatorward of ±40°. Finally, four terrain types were analyzed based on geologic maps by Scott and Tanaka (1986) and Greeley and Guest (1987).

3.5.2.2. Bimodal Nature

Stepinski *et al.* (2009) clearly showed *d*/*D* are bimodal for craters equatorward of ~±40°, the deep craters being "severely depleted southward of ~38°S." Their work was among the first to study this in a broad, systematic way, though they used a sub-set of 2444 craters to do so. Previous research dating to 1993 (Mouginis-Mark and Hayashi, 1993) used 109 fresh craters 20-40°S and found a general shallowing trend farther south, but their lack of large numbers of craters limited the spatial analysis and robustness of their work. Similarly, Boyce and Garbeil (2007) identified this feature by using a test population of 6047 craters throughout the planet. Mouginis-Mark and Hayashi (1993) attributed this to a cryosphere, and Stepinski *et al*. (2009) identified this as a possible contributor, as well. Stepinski *et al*. (2009) also raise the possibility of surficial mantling deposits as suggested by Soderblom *et al.* (1973, 1974). Boyce and Garbeil (2007) have a different interpretation. They suggest there is a gap in crater ages separated by the Late Noachian / Early Hesperian boundary that was the result of "abrupt onset and cessation of an episode of terrain degradation" as suggested by Craddock and Maxwell (1993). This would reflect a very rapid 10 μm/yr erosion/infill rate (current estimates are ~1-10 nm/yr (Golombeck *et al.*, 2006)). They suggest the contrast with higher latitudes indicate these erosion processes were not active there or other processes erased their effects.

Similar results are found in this database, as illustrated in Fig. **28**. Simple craters tended to have slightly deeper *d*/*D*, as would be expected from Section 3.5.1, so they are not plotted separately. In Fig. **28**, two different datasets are shown – the overall results for all craters as small red dots and craters with a degradation state of 4 as larger blue dots. An alternate definition of degradation state, only used in this analysis, removes the discriminator of depth/Diameter ratio (green dots). This work finds similar results as Boyce and Garbeil (2007) and Stepinski *et al.* (2009), but from a broader examination, more detail can be gleaned.

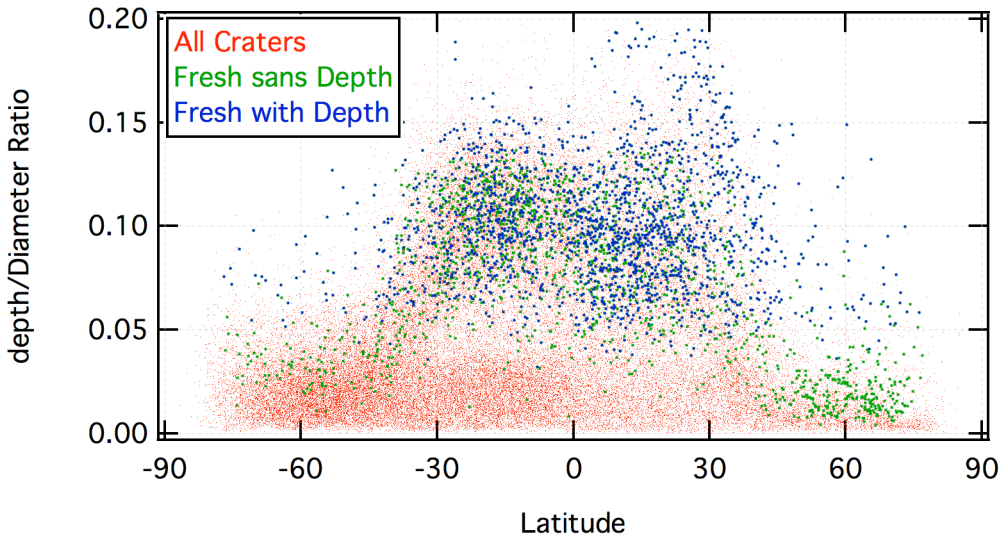

Figure 28: Scatter plot showing all craters with only fresh craters over-plotted. Red dots represent all craters, green symbols are fresh craters based only on morphology, and blue symbols are fresh craters that include depth/Diameter ratio as a parameter (craters in both sets will be blue).

First, the same pattern of a gradual *d*/*D* decrease in the deepest craters occurs over the ~10° range of ±30-40° latitude. However, the north and south hemispheres vary significantly in the magnitude of the difference. In the south, which is what previous works looked at (likely due to the larger crater population in that hemisphere), the *d*/*D* changes from a relatively tight distribution of ~0.0.8-0.14 and decreases to ~0.04 with outliers that go up to ~0.10. In the northern hemisphere, there is significantly more spread with *d*/*D* ranging from ~0.08 up to ~0.20. In the higher northern latitudes, there is a shift where a large number of craters are concentrated at shallow ~0.02 ratios but with a nontrivial number of craters as deep as ~0.05-0.10 at high northern latitudes.

Most of this is reflected well in the "all craters" population in Fig. **28**. The pattern is mirrored in the "Fresh sans Depth" population of craters; this is shown because, despite analysis in the next section, there may still be more significant terrain dependence than the deepest craters *d*/*D* relationship shows (there are 50% more fresh craters with this definition than with the full definition). The craters using the full definition of "Fresh" show similar patterns for equatorial craters but very few are present at higher latitudes.

There are several pieces of data that can inform the interpretation of these observed trends. This discrepancy between the northern and southern hemispheres can be partially explained by the presence of large impact basins and volcanic complexes in the northern hemisphere that contain the deepest craters on the planet (see Section 3.5.1). Though this can explain the differences up to ~30-40°, it is not adequate for the higher northern latitude discrepancy. A possible explanation is that the crustal thickness in the southern hemisphere may add strength to the rock, allowing it to support deeper crater cavities. In the north, the ice table may be both thicker and closer to the surface - indeed, *Phoenix* at 68.22°N found ice just a few centimeters from the surface (Smith *et al*., 2009). The enhanced relaxation cannot support deep craters, so even otherwise morphologically fresh craters are still comparatively very shallow. Another possible contributing factor could be that there is a more diverse terrain in the higher southern latitudes than in the north. In the north, the northern part of Tharsis and Utopia are present, but otherwise the terrain is predominantly the low northern plains and polar cap. The high southern latitudes contain major volcanoes, the southern half of the comparatively fresh Hellas and Argyre basins, southern highland terrain, and the residual polar cap. While these are offered as likely contributing factors, this should be an area of future investigation.

3.5.2.3. Deepest Craters Method

Arguably, measuring the deepest, freshest craters is likely to produce the best estimate of the original, pristine, just-after-formation crater depth-to-diameter ratio. This method has been utilized in the past several times, notably by Garvin *et al.* (2003) and Boyce and Garbeil (2007). The former used the deepest 25% of their simple craters from which they estimated a $d = 0.21D^{0.81}$ relationship from 469 craters for $D \leq 6$ km, and $d = 0.36D^{0.49}$ for complex craters $D > 6$ km. The latter examined craters $12 \leq D \leq 49$ km and found a relationship of $d = 0.315D^{0.52}$, in reasonable agreement with Garvin *et al*. (2003).

The methodology of Boyce and Garbeil (2007) is what was used here: They separated craters into diameter size bins and then iteratively used the single deepest, average of the two deepest, average of the three deepest, etc. craters in each bin through which to fit a power law.

They found the slope of the power law was a constant 0.52±0.004 despite increasing the number of craters, while the amplitude of the power law fit changed from 0.363 to 0.356 to 0.333, decreasing with increasing numbers of craters. This was expected and helped to confirm they were sampling the results of the underlying physical process rather than secondary effects, and it produced a more robust result. The value quoted above is for the five deepest craters.

Repeating their example, craters from this database were binned in multiplicative $2^{1/8}D$ bins. Larger intervals were used, where the deepest two craters were averaged together and a power law fit, then the deepest 3, 4, 5, 10, 15, 20, and 25 per bin. For complex craters $6 < D < 90$ km, the exponent reached a constant level for 3 or more craters with a range of $0.572 - 0.593$ and mean 0.582±0.008. While this is slightly greater than their value, it is still fairly close and can be explained because of the use of a larger dataset and diameter range. Also similar to their results, the amplitude started large at 0.360 and proceeded to decrease linearly when including 4 or more craters ($A = -0.0025N + 0.2938$ where A is the amplitude and N is the number of craters). While a smaller amplitude is reported here than in Boyce and Garbeil (2007), this can be explained in that their definition of crater depth was average rim height to the deepest pixel on the floor; the definition used in this database was average rim height and the average of many floor pixels (at least $N = 3$).

The analysis for simple craters was not as straight-forward. The exponent on the fit varied significantly until at least four craters were included, at which point the range was $0.985 - 1.038$ with a mean 1.012 ± 0.020. This is steeper than Garvin *et al.* (2003) and likely represents a larger dataset over a broader region of the planet (global) from their work. The robustness of this exponent in other analyses in this work indicates it is likely not anomalous. The amplitude of the fit decreased dramatically from a maximum of 0.271 to an average of 0.179 ± 0.001 for the 10-25 deepest crater fits.

Based on this work, the averages are what will be quoted as the "final" values for the global depth/Diameter relationship on Mars for these craters and they are reported in Table **5**. The amplitude from the 4 deepest craters fit for complex craters is used because that was the

onset of an observed linear decline. When exploring this further, the craters were separated into regions – northern plains, southern highlands, polar, and volcanic – and separated by latitude – equatorward of ±40°, and poleward of ±40°. The regressions were again run, and the results are found in Table **5**.

When examining the craters poleward of ±40° latitude, in both simple and complex crater cases there was no convergence upon a single value for either the exponent or amplitude of the fit for simple and for complex craters. This may be due to relatively small number statistics, but there were still several thousand craters being analyzed and this is an unsatisfying and unlikely

Table 5: Crater depth/Diameter ratios on Mars have been quoted as overall global averages for decades, but examination of the global distribution shows there are variations based on terrain. This table shows the simple (top line) and complex (bottom line) depth/Diameter relationship when are divided into a variety of terrain types. The number *N* of craters in this table is the number used in the "All Craters" analysis.

		Deepest Craters	Fresh Craters	All Craters
Global	Smp (N = 37,091):	$d = 0.179D^{1.012}$	$d = 0.097D^{1.061}$	$d = 0.047D^{1.284}$
	Cpx (N = 32,021):	$d = 0.286D^{0.582}$	$d = 0.250D^{0.527}$	$d = 0.107D^{0.559}$
-40° to +40°	Smp (N = 24,875):	$d = 0.175D^{1.022}$	$d = 0.084D^{1.245}$	$d = 0.078D^{1.106}$
	Cpx (N = 22,290):	$d = 0.280D^{0.570}$	$d = 0.229D^{0.567}$	$d = 0.155D^{0.464}$
≤-40°, ≥+40°	Smp (N = 12,210):	$d = 0.177D^{0.724}$	$d = 0.083D^{1.073}$	$d = 0.014D^{1.465}$
	Cpx (N = 9742):	$d = 0.244D^{0.579}$	$d = 0.174D^{0.629}$	$d = 0.032D^{0.881}$
Northern Plains	Smp (N = 3693):	$d = 0.165D^{1.094}$	$d = 0.073D^{1.311}$	$d = 0.011D^{1.992}$
	Cpx (N = 1308):	$d = 0.479D^{0.359}$	$d = 0.274D^{0.502}$	$d = 0.227D^{0.158}$
Volcanic Terrain	Smp (N = 2471):	$d = 0.212D^{0.886}$	$d = 0.182D^{0.718}$	$d = 0.091D^{1.010}$
	Cpx (N = 1008):	$d = 0.291D^{0.526}$	$d = 0.240D^{0.539}$	$d = 0.209D^{0.451}$
Southern Highlands	Smp (N = 23,087):	$d = 0.235D^{0.777}$	$d = 0.154D^{0.821}$	$d = 0.051D^{1.261}$
	Cpx (N = 23,850):	$d = 0.303D^{0.571}$	$d = 0.231D^{0.556}$	$d = 0.112D^{0.541}$
Polar Terrain	Smp (N = 727):	–	–	$d = 0.0028D^{1.843}$
	Cpx (N = 202):	–	–	$d = 0.014D^{1.161}$

reason. To extend the trend, additional regressions with 30 and 50 deepest craters were calculated. For simple craters, a trend emerged with $N \geq 10$ craters for the exponent to be $p = 0.014N + 0.667$. Similarly, a line could be fit for the amplitude $A = -0.013N + 0.237$. Since it is for $N = 10$ craters that a predictable pattern emerged, it is those values quoted in Table **5** and used in determining crater degradation state for this latitude range (see companion paper, this volume). A similar pattern was present for $N \geq 5$ craters for the complex regression, $p = 0.038N + 0.448$ and $A = -0.023N + 0.313$. Thus, it is the $N = 5$ regressions quoted in Table **5** and used to determine crater degradation state.

This indicates that, as expected from Section 3.5.2.1, craters are shallower overall at higher latitudes. This must be taken into account when utilizing *d*/*D* as a proxy for crater degradation state, for it will result in anomalously degraded craters at these latitudes. Of interest, the complex slope is very similar to that for the globe, but the slope for simple craters is significantly shallower. This is likely due to two main reasons. First, as identified in Boyce *et al*. (2006) and discussed in Section 3.5.1, the very deepest and largest simple craters are in Chryse, Utopia, and Isidis, generally south of 40°N latitude; while these will be included in the global analysis, their absence here will decrease the amplitude of the largest few diameter bins and hence decrease the exponent. Related, the second likely contributing factor is that the crustal strength is significantly less, and the inability to support deeper cavities will likely scale with crater diameter, also decreasing this exponent. It should be noted, however, that the slope calculated here is very similar to the simple crater relationship calculated by Garvin *et al*. (2003).

While the relationship poleward of ±40° was subject to significant differences, perhaps unsurprisingly the relationship equatorward of ±40° was very similar. This is easily explained by the deepest craters being in this region of the planet and so an algorithm designed to capture the deepest ones would pick up on these in a global distribution. Regressions over the same *N* range as for >±40° were run with the simple craters converging for $4 \leq N \leq 30$ craters per bin, with the exponent 1.022±0.021 and amplitude 0.175±0.002. Complex craters did show a slight decrease in slope as *N* increased beyond 5, but the magnitude of this decrease was <8%. The

average over $10 \le N \le 30$ was 0.570±0.010 and the amplitude 0.280±0.001. Overall, these results are in good agreement with the global average and are within the quoted ranges.

Analysis by terrain type for the deepest craters method yielded higher amplitudes for the complex crater *d*/*D* relationship for all three analyzable terrains - northern plains, volcanic terrain, and the southern highlands. (Polar craters numbered too few to be analyzed with this method.) The difference was greatest in the northern plains where the amplitude was fully 67% greater than the global function. However, the exponent was significantly shallower, only 62% of that for the global relationship. This would indicate that smaller craters start out deeper in the northern plains but then do not increase in depth as rapidly. Similarly, the exponent on the simple crater function for the volcanic terrain and southern highlands was shallower while the amplitude was just slightly higher, indicating a similar trend as with complex craters in the northern plains.

3.5.2.4. Fresh Craters Method

Recent work to define the *d*/*D* relationship for Mars (*e.g.*, Garvin *et al.*, 2003; Stewart and Valiant, 2006) has generally relied upon identifying and measuring the depth and diameter values of morphologically fresh/pristine craters. The Garvin *et al*. (2003) results are described above and agree generally well with the deepest crater method. Stewart and Valiant (2006) limited their analysis to five regions on Mars and examined relatively few craters in each: Acidalia Planitia ($N = 29$), Utopia Planitia ($N = 53$), Isidis Planitia ($N = 24$), Lunae Planum ($N = 48$), and Solis Planum ($N = 33$). Utopia and Isidis were identified previously in this work, Boyce *et al*. (2006), and Stepinski *et al*. (2009) as having deeper craters than the average terrain, and they found deeper *d*/*D* when just looking in those regions ($d = 0.404D^{0.41}$ for Utopia and $d = 0.351D^{0.41}$ in Isidis). Acidalia is north of the Chryse impact basin and is around the region identified above as also having deeper than average craters, and they identified a relatively deep crater relationship there, as well, of $d = 0.384D^{0.38}$. Interestingly, the slopes in all of these relationships are shallower than identified by the work from this crater database, indicating that they found, by comparison, either smaller craters to be deeper or larger craters to be shallower.

Another possible explanation is that there may be relatively large uncertainties due to the comparatively small number of craters in their study.

The analysis in this section mimics this approach and only uses craters that are classified with a degradation state of "4" (fresh). This process is slightly incestuous because one of the four parameters in crater degradation state is the crater depth relative to the established d/D relationship. To minimize how recursive this process is, the deepest crater d/D was used to define that part of crater degradation state such that this fresh crater method could be relatively independent. Overall, 2704 craters $D \geq 5$ km were identified as "fresh" in this database. Of those, 934 were classified as simple (831 were equatorial of ±40° and 103 poleward), and 1060 were complex (976 were equatorial of ±40° and 84 were poleward).

As an overall global average, the slope of the fresh simple and complex craters was similar to the deepest crater method, varying at the few-percent level and likely within the noise. The amplitude of the fit is expectedly smaller than the deepest crater method, though the difference is roughly a factor of $2\times$ for simple craters but only ~15% for the complex craters. This is easily explained in that the fresh craters method is sampling an ensemble of terrains (the whole planet) and that the deepest crater method is simply picking the deepest ones which have been shown to be terrain-dependent. The relative lack of a difference at the larger, complex crater diameters can be interpreted as these craters are less dependent upon terrain type than smaller craters and therefore there are fewer deepest craters that then get averaged out.

Regressions were again run for the sub-regions, and the results are shown in Table **5**. Overall, the separation by latitude range is similar to the trend found for the deepest craters, though it should be emphasized that small numbers towards the poles ($N = 103$ for simple and $N = 84$ for complex) may limit the robustness of the fits. Analysis by terrain type could not be done for the polar terrain craters because the numbers were too small. Overall, the terrain separation did not yield significantly different results than the global analysis except in three values. First, the exponent in the simple crater fit for the northern plains was substantially steeper than both the global average and equatorial range. Second, the amplitude for the simple

craters in volcanic terrain was twice that of the global average and the latitude separations, indicating that simple craters start substantially steeper in volcanic terrain, but the exponent was smaller, indicating that as they increase in diameter, the depth does not grow correspondingly as large as for the global average.

3.5.2.5. Average Across Crater Depths and Degradation States

An additional method that may have dubious intrinsic physical meaning is that of taking an overall average of depths of craters for a given diameter. This was done in Stepinski *et al.* (2009) to define $d = 0.025D^{1.6}$ for simple craters D < 7 km, and $d = 0.22D^{0.47}$ for complex craters $D \geq 7$ km based on a combined total of 3666 craters. Earlier, Garvin *et al.* (2003) produced overall average results for simple craters $D \leq 6$ km of $d = 0.21D^{0.80}$ from 2263 craters. This is only slightly different from their results for the deepest craters, and it is significantly different from the Stepinski *et al*. (2009) function.

Fitting was done in the same manner as the previous sections, and results are reported in Table **5**. In this case, *all* craters were included in these numbers rather than the deepest or freshest. Globally, the complex crater function was similar in slope to the overall average, though it was slightly shallower, and the amplitude was 37%. This indicates that as a whole, Mars' crater population has been infilled/modified relatively evenly across diameter ranges, though there may be slightly more infilling at larger sizes. This is interpreted as larger craters are generally older and so would be more infilled on average than a broader age range at smaller diameters. The simple crater population is significantly different, for it has an amplitude of 26% the deepest craters but an exponent 27% greater. Borrowing from the above interpretation of exponent differences in complex craters, this indicates that more small simple craters are significantly infilled than larger ones. While this may be the case, it could also be an artifact of the MOLA data used in this analysis as discussed in the companion paper (Robbins and Hynek, 2011b) and the beginning of this section. Further work examining each crater with MOLA shot data and/or comparison with higher resolution DTMs are necessary to resolve whether the latter issue is a significant factor. Both of these are significantly different from Stepinski *et al*.'s

(2009) results.

Division of the craters along the ±40° latitude lines resulted in somewhat different results to those found in Section 3.5.2.3 with the deepest craters. In regions poleward of ±40°, the amplitude of the fits decreased by a factor of $\sim 3\times$, while the amplitude of the fits for craters equatorward of ±40° increased by a factor of $\sim 1.5\times$. Interestingly, the exponents underwent the opposite, where the equatorial craters' exponents dropped by ~20% while the polar simple craters rose by 14% and complex by 58%. This was the steepest complex crater relationship found in this work except for the polar terrain separation. Interpretation of these results for amplitude is straight-forward and discussed above, for polar craters are shallower because of a weaker crust likely due to a cryosphere. The exponents are a different matter, and most significant are the poleward results. The hypothesis discussed above that the anomalously large exponent for simple craters may be due to MOLA artifacts should be less significant near the poles because of higher point density due to the *Mars Global Surveyor* orbit; thus, these results should be *more* robust than their equatorial counterparts, but the slope is greater. If this is a real phenomenon, this would indicate the former interpretation for the global results is more likely, that smaller craters are more infilled than larger ones, which would seem to belie a normal sequence of events: larger craters preferentially form earlier on a surface while more smaller craters form later, and assuming an even rate of infilling/erosion, the d/D slope should remain fairly steady while the amplitude decreases. More work on this issue should be done to unravel this result.

The all-crater average when craters were separated by terrain yielded a few interesting results. First, the polar terrain craters could be analyzed with this method, and as expected they were significantly shallower than the global average. The simple craters' fit function had an amplitude of 6% the global and the complex was 13%. However, the power law exponents were significantly steeper by 43% and 107%, respectively. This can be explained by the proposal in Section 3.5.1: Smaller craters will feel the effects of the terrain much more than larger craters. Thus, the polar terrain will cause a significantly shallower crater, but as craters get larger the terrain dominance lessens and normal gravity scaling dominates more. Otherwise anomalous

were the craters on volcanic terrain with amplitudes a factor of 2× greater than the global average. However, this can be fairly easily explained by fresh craters dominating Martian volcanic terrain (64% are degradation states 3 or 4) and so more modified, shallow craters do not lower the average.

3.5.3. Synthesis of the depth/Diameter Relationship

Crater depth/Diameter relationships are an important tool to understanding how craters form and then how craters differ from what is expected. Investigation into this relationship was done in three main ways – deepest craters, fresh craters, and all craters – and investigated for the entire globe, different latitude bands, and specific terrain types. Overall, the results are reasonably consistent with most previous work in this area (*e.g.*, Garvin *et al.*, 2000, 2003; Stewart and Valiant, 2006; Boyce and Garbeil, 2007) though it varied from the automated analysis of Stepinski *et al*. (2009).

The work presented here was incremental in revising these relationships: Within the nineteen different method-region combinations for both simple and complex craters, the results were generally self-consistent. Significant variations were generally expected due to the particular analysis conducted. For example, the deepest craters method consistently yielded the deepest d/D relationship while the all-crater averages were always the shallowest. The exponent slopes were also generally consistent among each other, though a few outliers did exist as explored in the previous subsections. Overall, though, it is reassuring that the different methods yielded similar results with most differences easily explained. This is the first work to examine these relationships through multiple methods and compare them.

The application of this analysis to future research should probably be limited to using the deepest craters method results when separated by terrain type. If a crater is emplaced in a terrain that was not covered by the four major ones analyzed here, then researchers should use the latitude bands. Using the global average will result in underestimating original crater depth in some cases such as on volcanic terrain, or overestimating original depth in locations such as near

the poles.

3.6. The Simple/Complex Morphology Transition and Gravity Scaling

Simple craters are small and bowl-shaped while complex craters are large and have a variety of interior morphologies such as wall terraces, central peaks, and flat floors. Fundamentally, the transition diameter between simple and complex craters has been observed to be a function of the surface gravity of the target object (*e.g.*, Baldwin, 1949; Quaide *et al*., 1965; Malin and Dzurisin, 1977; Pike, 1977). However, it is also at least in part controlled by target material strength (*e.g.*, Pike, 1980; Pike, 1988). Determining the diameter at which an impact crater will transition from simple to complex morphology can inform studies of the target, its properties, and the role of gravitational collapse and elastic rebound. These are the main mechanisms during crater formation's modification phase that produce complex morphologies. While the diameter of this transition is necessarily a range because different morphologies will be begin to form at different diameters, the diameter of this transition was found to be roughly 6 km for Mars with no significant terrain dependence (Pike, 1988). This value has been argued about over the years with each new dataset of craters, and in that tradition this database was mined to determine if Pike's 1988 conclusion should be revised.

3.6.1. Based on Floor Shape

A crater is considered to be within the basic complex type when it displays a flat floor morphology that is not due to post-formation infilling. Additional features are often characteristic of complex craters, but these are addressed in subsequent sections. To the goal of discerning the average diameter transition from simple to basic complex morphology, all craters in the database (Robbins and Hynek, 2011b) were classified - if possible - into these basic types. Craters in the ~5-8 km-diameter range were not classified if it was not clear if they were either pristine complex flat-floored craters or infilled (modified) simple craters.

Three histograms were created to quantify this: all craters, all simple craters, and all complex craters. The simple and complex crater histograms were then divided by the overall database

histogram, and these are displayed in Fig. **29**; the sum of the two is also shown. The simple-complex transition diameter is where the fraction of complex craters is greater than simple craters, and it is 6.9 km (Fig. **29**). This diameter proved to be robust when separated into two latitude ranges – ±40°, and poleward of ±40° – the equatorial band having a transition location of 7.0 km and 6.9 km for the polar (well within any reasonable uncertainties). Examining craters at higher latitudes, however, yields interesting results: Poleward of ±60°, the transition occurs at 7.7 km, and at >±70°, it rises to 8.0 km (this is fairly robust as there are still >1000 craters in the database around the diameters of interest). Separating these by northern and southern hemispheres yields a transition at 8.1 km for <-70°N, and those >+70°N have a transition ~8.4 km. A similar effect was found when separating by terrain type as in Section 3.5.2: Polar terrain craters had a transition of ~7.9 km while the other three (northern plains, southern highlands, and volcanic) were ~7.0 km. This is similar to findings by Garvin *et al*. (2000).

The dependence upon latitude and terrain has not been quantified before. As discussed, the transition is a consequence of collapse under gravity due to surpassing the strength of the tar-

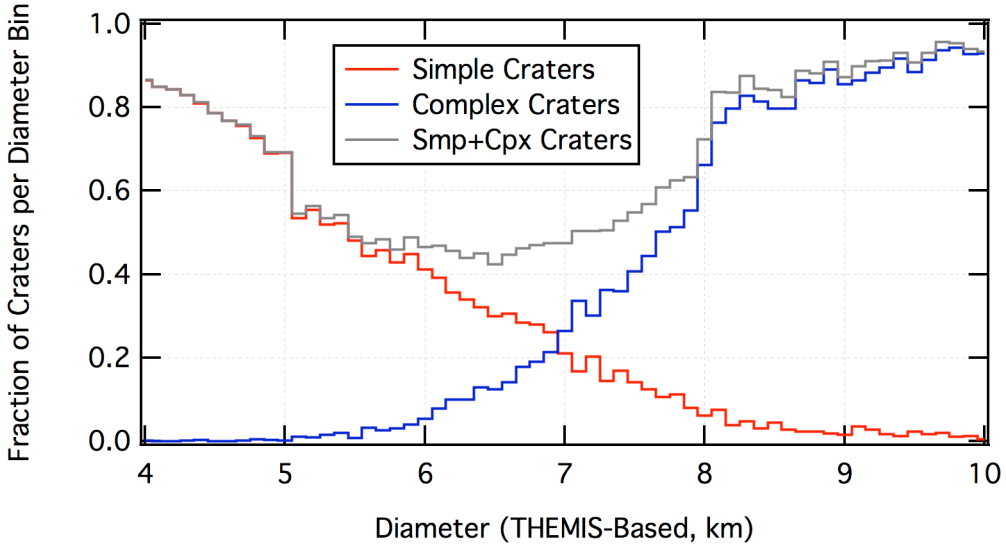

Figure 29: Three histograms were created as a function of diameter: All craters, simple craters, and complex craters. The simple and complex crater histograms were divided by the histogram for all craters and are plotted here, their sum shown in grey. The deficit relative to 100% of all craters being classified between ~5-8 km is due to the conservative classification to avoid classifying infilled simple craters as flat-floored pristine complex craters and vice-versa.

get. This runs contrary to what one would expect for the Martian crust for, as graphically illustrated in Section 3.5, the higher latitudes of the planet are likely dominated by a near-surface cryosphere (Boynton *et al*., 2002) and the cryosphere at northern latitudes is probably closer to the surface (Section 3.5.2.2). From this, one would expect an impact into an ice-solidified crust would vaporize volatiles and weaken the crust, permitting gravitational collapse to a complex crater at smaller diameters rather than strengthening it for transitions at larger diameters. A possible explanation is that water in the surface causes it to act more fluid during the modification phase of crater formation. The result will be material gently sloping down the crater walls, shallowing the bowl, but maintaining the bowl shape and thus resulting in a simple crater classification.

3.6.2. Based on Other Complex Crater Morphologies

Expanding on the morphologic method to examine transition diameter is by looking at what diameter range other complex crater morphologies begin to form. Although Pike (1980, 1988) examined several morphologies (flat floor (addressed above), central peak, scalloped rim, terraced wall, ballistic ejecta, flow ejecta), in this analysis the morphologies are limited two to additional ones – central peaks and terraced walls. Central peaks form by rebound of the crust during crater formation. Terraces are a collapse feature from the walls during crater formation. While these are fundamentally different processes, and they will manifest at different crater sizes, they are each a good morphologic indicator of failure of the crust to support a simple bowl and hence display a complex crater. Craters were binned similarly as in the basic morphology, discussed above. An average was taken at the diameter where the fraction of the craters that contained the feature was stable. Then, the diameter at which 50% of the average was reached was considered the transition diameter.

Central peaks were present in an average of 6.3% for crater diameters $D \geq 15$ km. 50% of this - where 3.2% of the craters had central peaks - was reached at $D = 5.6$ km. The smallest crater with a central peak was ~2 km, but it did not reach the 5% steady-state level until $D \geq 3.3$

km. Performing the same analysis on equatorial craters shows a smaller diameter transition D = 4.8 km, while the >±40° latitude range yielded a larger diameter of 11.3 km. Similar results were found on volcanic and southern highlands terrain while there were not enough craters for an analysis on polar. The northern plains, however, were significantly different with a transition to central peaks at D = 8.4 km.

Terrace morphology did not reach a steady state until $D \approx 15$ km, and this was at a level of 21%. 50% of this was reached at D = 8.3 km. The smallest crater with wall terraces was ~3 km, but it did not reach 5% of steady-state until $D \geq 4.5$ km. Performing the same analysis on equatorial craters shows a slightly smaller diameter transition of D = 7.5 km, while the >±40° latitude range yielded a significantly larger transition diameter of 16.9 km. Terrain-dependent results were similar to the global average except for polar where again small numbers made this analysis difficult; the smallest diameter crater with visible terraces on polar terrain was 10 km.

These values are in rough agreement with Pike (1980) who found transition diameter from central peaks and terraces to be in the 6-8 km-diameter range with the prevalence of wall terraces at larger diameters than central peaks (he found a difference of a factor of $2\times$, though this work and methodology shows it to be $1.5\times$). The latitude range-dependent trend observed here supports the idea from flat floor morphology that it is more likely this is a real feature of the craters rather than an error in classification.

Issues with erosion of these more complex features are likely significant, for one would expect the vast majority of larger complex craters form with terraced walls and likely central peak features from basic cratering physics (Melosh, 1989). For example, when only examining fresh craters, terraces were identified in >90% of craters $D \geq 20$ km, and central peaks were present in 55% of $8 < D < 13$ km craters and >90% of $D > 14$ km craters. However, erosion should affect these features relatively evenly across the crater diameters, so this should not significantly affect results (Craddock *et al*., 1997).

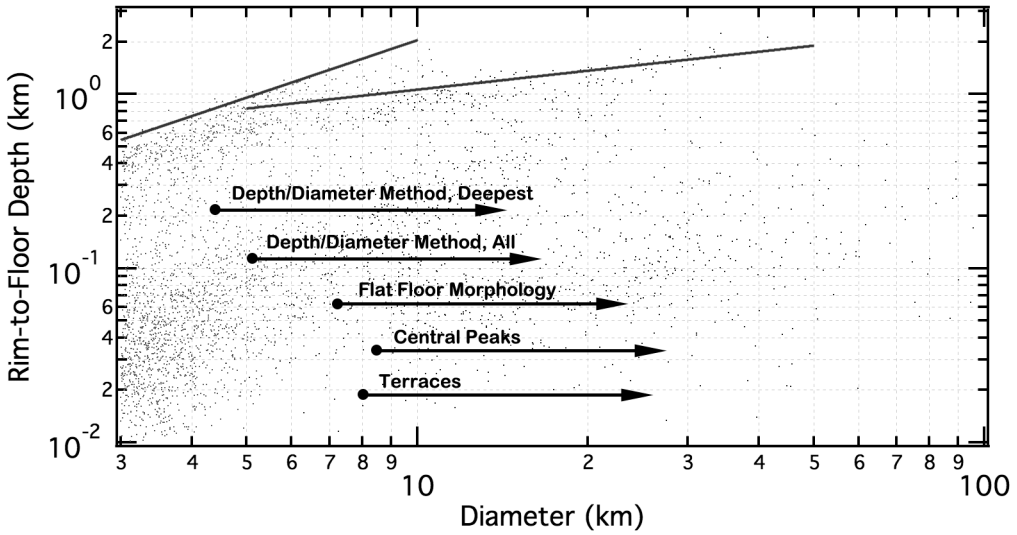

Figure 30: Simplified diagram illustrating the diameter at which the simple-complex transitions are observed for the northern plains. Dots are craters, and the two crossing lines are the best-fits for simple and complex deep craters. Arrows indicate the transition diameter from simple to complex for each of the labeled characteristics examined. Vertical offset is arbitrary.

3.6.3. Based on depth/Diameter

A more common method of determining transition diameter is on a crater depth versus diameter plot (*e.g.*, Fig. **30**). On these, simple craters will have a relatively steep slope compared with complex craters, and there will be a "knee" where they intersect. Some overlap is present due to target, impactor, and other variances, but in general this occurs over a narrow diameter range. Indeed, when fitting the slopes to a power law function (Section 3.5.2), there is an exact diameter at which the slopes intersect. This diameter is what is used and reported in this section.

Globally, for the deepest craters method, the transition diameter is 3.0 km. The fresh crater method puts the transition at 5.9 km, while the all-crater average is 3.1 km. Transitioning to the equatorial latitude band, the diameter goes down slightly for all cases - following the pattern in the previous two sections - to 2.8 km, 4.4 km, and 2.9 km. The higher latitudes saw mixed results with a spurious 9.2 km result for the deepest craters method due likely to small numbers, 5.3 km for the fresh method, and 4.2 km for the global average. Overall, these are nearly all smaller than the simple-to-complex transition diameter than when based upon morphology alone. This phenomenon was observed in previous work by Pike (1988) not only on

Mars, but also on Earth, Mercury, and the Moon. A figure similar to his Fig. 11 is shown as Fig. **30**, illustrating this point as well as showing the general diversity of the onset of these morphologic and morphometric characteristics.

3.6.4. Synthesis of the Simple/Complex Morphology Transition

Overall, this is the first work to utilize a modern global crater database to re-examine the simple-complex morphology transition on Mars. It does so with respect to multiple morphologic and morphometric indicators and a latitude and terrain dependence. The results of this analysis of independent morphologic and morphometric transitions are summarized in Fig. **31** and Table **6**. Only the transition diameters for the deepest craters *d*/*D* relationship are used to calculate the arithmetic and geometric means (except for polar terrain). These means are very close to each other, and the standard arithmetic would normally be used but Pike (1988) used geometric so that is included as a comparison. The means for the global distribution are 6.0 km average and 5.6 km geometric; the standard deviation is ±2.3 km. Pike (1988) calculated ~6 km for the transition. The other results are in Table **6**.

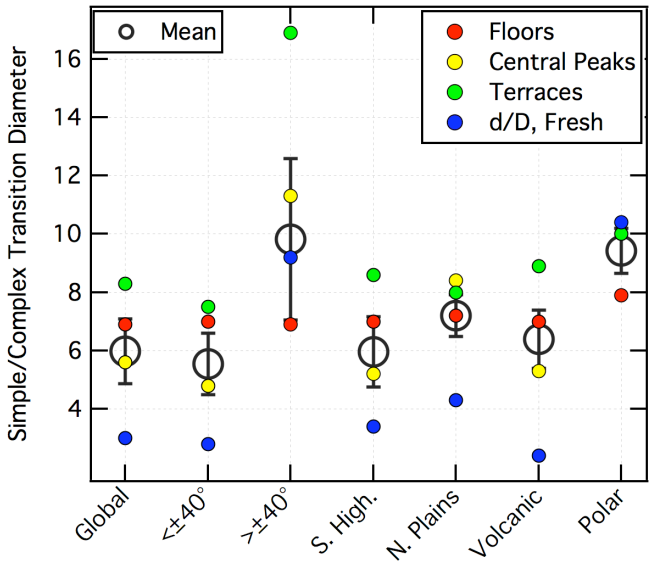

Figure 31: Combined results from using different morphologic and morphometric indicators to determine the transition between simple and complex crater morphology on Mars. Solid circles are points showing each result discussed in the text, the key to which shown by the legend to the upper right. Black open circles are the arithmetic means for all morphologic data and results from the deep crater *d*/*D* method (since that is considered the most robust technique (see Sections 3.5.2 and 3.5.3)). Error bars are the standard deviation from the means of the three or four values divided by $\sqrt{N}$.

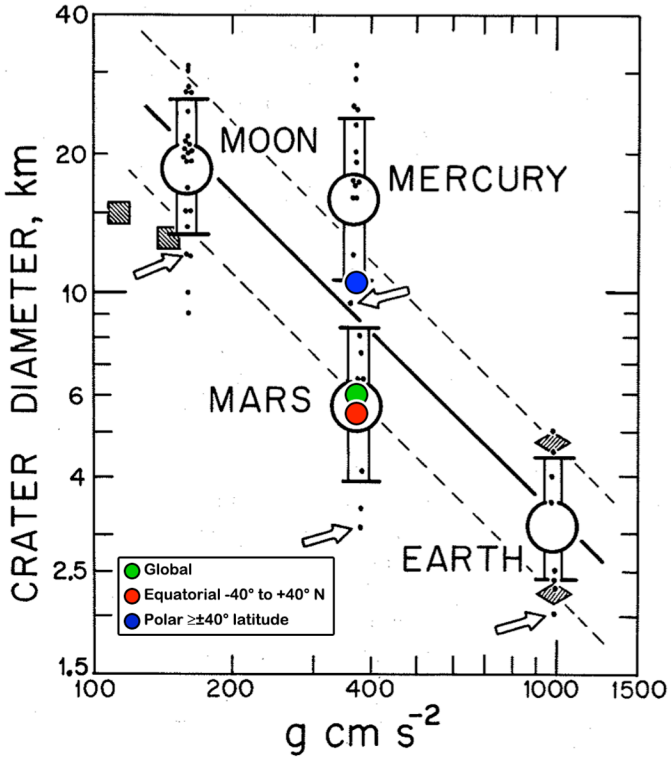

Figure 32: Background Figure is from Pike (1988, reproduced without permission), illustrating surface gravity versus onset of complex crater morphology for the large inner solar system bodies (except Venus) and Ganymede and Callisto (squares). Each small black dot is from Pike (1988) and represents a different morphologic indicator (*e.g.*, the previous subsections); he analyzed 230 Martian craters. Arrows point to *d*/*D* results. Large circles are geometric means and bars are standard deviations. The solid black line is a best-fit, while the diamonds are for different targets on Earth and the dashed lines extrapolations of the fit for those targets (lower is for sedimentary rock, upper is crystalline). Overplotted in color are the results from this work (arithmetic means).

Table 6: Summary of transitional diameters for different Martian terrains and derived through various means discussed in the text (all units are km).

	Global	<±40°	>±40°	S. High	N. Plains	Volcanic	Polar
Floors	6.9	7.0	6.9	7.0	7.2	7.0	7.9
C. Peak	5.6	4.8	11.3	5.2	8.4	5.3	–
Terr.	8.3	7.5	16.9	8.6	8.0	8.9	10.0
d/*D*, Deep	3.0	2.8	9.2	3.4	4.3	2.4	10.4[1]
A. Mean	6.0	5.5	11.1	6.1	7.0	5.9	9.4
G. Mean	5.6	5.2	10.5	5.7	6.8	5.3	9.4
Std. Dev.	2.3	2.2	4.3	2.2	1.9	2.8	1.3

[1]There were not enough craters to derive a reliable function for the "deepest" crater method for polar terrain craters. The "all-craters" method value is quoted in its stead, and it was used to compute the averages and standard deviation.

This work supports Pike's 1988 analysis from *Viking* imagery that indicated different transition diameters for different simple/complex morphologies, as is indicated by the overlap shown in Fig. **32**. It is, however, significantly more robust, utilizing thousands of craters across the globe instead of 230 craters. It used a variety of modification states as well as and only fresh craters as a check. The global results fit very well within Pike's synthesis and lie directly upon the lower dashed line of Fig. **32** that indicates similarity with sedimentary rock on Earth.

Of particular interest, though, is the latitude and terrain dependence shown. This result was robust in the previous sections: The equatorial range of <±40° latitude showed slightly smaller transitions while the polar range was significantly larger for nearly all morphologic and morphometric indicators (though the ranges do slightly overlap, as shown in Fig. **31**). The observational implication is that crust in the equatorial band of Mars is less competent and craters will undergo gravitational collapse during the modification phase of formation more readily. By the same token, the northern plains consistently had significantly larger transition diameters and the means are correspondingly greater. Meanwhile, the crust closer to the poles is more competent and less prone to this form of collapse. Interestingly, this runs contrary to the basic interpretation of crater depth/Diameter data discussed in Section 3.5. That indicated the crust was weaker near the poles because even morphologically fresh craters were a factor of $\sim 2-3\times$ shallower than their equatorial counterparts. These disparate relationships are addressed in Section 3.7.

3.7. Discussion and Conclusions

We have explored the basic crater distributions, morphologic distributions, morphologic relationships, and morphometric relationships from a new global crater database of Mars. This database was shown to be statistically robust (companion paper, this volume), and we examined many previously known trends to illustrate its agreement with previous work. We also expanded the analysis to illustrate the utility in discerning new trends and relationships as well as to refine some that have been studied for decades.

In basic crater distribution across the planet, we illustrated this database is coincident with previous research in global distributions and age-related trends. Expanding this to smaller diameters illustrates significant new work and forms the bulk of the number of craters in this database. The small crater population shows finer age variations across the surface in contrast with the 5-50-km-diameter population, and it also starts to inform studies of secondary crater populations (Robbins and Hynek, 2011a; Robbins and Hynek, 2011d). A new analysis comparing the fresh crater population with global circulation models of the planet agree well, and future work may yield tighter constraints or inform other processes that may protect craters from aeolian erosion.

Our work examining crater interior morphologies (central peaks, summit pits, and central pits) provides validation of our database, updates older results (*e.g.*, Barlow and Bradley, 1990), and extends other modern ongoing work to the southern hemisphere (Barlow, 2010, 2011). Central peak distribution generally correlates with fresh craters, but there is disagreement at central longitudes in the southern hemisphere. Further efforts in understanding this should be fruitful, as will further exploration into the distribution of Martian central pits and summit pits. The terrain in which these latter features are found supports a model that incorporates volatiles in their formation, though the specific model is open to interpretation from our cursory analysis (*e.g.*, Wood *et al*., 1978; Croft, 1981; Senft and Stewart, 2008; Alzate and Barlow, 2011). Morphometric analysis may support this and is underway by other researchers (Barlow, 2010, 2011; Alzate and Barlow, 2011). We examined the intracrater dune distribution, comparing it to the Mars Global Digital Dust Database (MGD^3) (Hayward *et al*., 2007; Hayward *et al*., 2008; Fenton and Hayward, 2010). In general, good agreement was found between our catalog and theirs, with small differences the subject of future collaboration. The largest difference was the inclusion of $\sim 4\times$ more dunes at latitudes 30-65°N in this catalog.

The distribution of radial ejecta was found to reproduce terrain ages reasonably well despite the craters forming after the terrain, illustrating that radial ejecta can be preserved over long periods of geologic time on Mars. Layered ejecta blanket data is abundant within the

database, comprising nearly 50% of the data columns with ejecta morphology and detailed morphometry. Extensive mining of this data for purposes of better explaining these features and their formation is the subject of future work in prep., but in this paper we showed its general agreement with previous work in the area (*e.g.*, Mouginis-Mark, 1979; Schultz and Gault, 1979; Barlow and Bradley, 1990; Barlow and Perez, 2003; Barlow, 2005) and demonstrated its utility in refining previous distributions and trends.

Our database provides detailed topographic information about craters, and this has resulted in updating some of the basic scaling laws as applied to Mars. Overall, we found that Martian craters display rim morphometries that are $\sim 2\times$ smaller than their lunar counterparts reported in Melosh (1989). This is the case for rim height and surface-to-floor depth each relative to crater diameter, and these hold for both simple and complex crater morphologies.

In further application to fundamental scaling, we examined crater depth-to-diameter ratios (d/D) as an incremental update to previously identified trends and values, though this was the first analysis to compare three different methods from the same dataset for deriving the d/D relationships on Mars. We illustrated the known global dichotomy of deeper craters in equatorial regions and shallower craters towards the poles, and we expanded upon this to show a previously unobserved secondary effect of a North/South dichotomy. This shows a wider variation of crater depths towards the equator in the north compared with the south, but the opposite was the case at polar latitudes. The high northern latitude craters showed a very tight and shallow distribution of depths compared with the south, likely indicating a nearer surface cryosphere and more uniform terrain. We reexamined the basic crater d/D relationship, as well, for both the global average and subregions. Within each, we characterized d/D for simple and complex craters in terms of the deepest craters, fresh craters, and all craters. Our results for the global average compare well with previous work, and our results within the terrain dependence reflect the dichotomy observed before. These differences are important, and they must be taken into account when using crater depth to estimate erosion, infilling, and other modification processes. Otherwise, one will interpret all high-latitude craters as degraded relative to equatorial ones.

These *d*/*D* results were then placed into the context of one of the other basic crater scaling laws of at what diameter does a crater transition from simple to complex morphology in a method similar to what has been done in the past (*e.g.*, Pike, 1977, 1980, 1988). Three morphologic indicators were examined - basic morphology (bowl vs. flat floor), central peaks, and wall terraces - and the intersection of the *d*/*D* fits were our morphometric criterion. We again segregated by terrain as well as examined the global relationship. Our results agree very well with Pike (1988) for the global population, and this lends credibility to the incredible difference observed between latitude bands: We found the simple-complex transition occurs at ~11 km at high polar latitudes rather than the ~6 km global average (Fig. **31**).

Taken with the *d*/*D* information, we propose a model where the higher latitude craters will begin to form as they do elsewhere through the contact and excavation stage. During excavation, the impact energies will melt and vaporize ices in the surrounding crust. This will weaken the crust where vaporized, and intense ground movements cause the wet crust to flow like mud. During the modification phase, the crust is not strong enough to support the deep cavity characteristic of equatorial simple craters, but the viscous fluid-rich material will relax, decreasing the crater depth but maintaining a bowl shape. A central peak, generally the first complex morphologic indicator, does not form until $D \sim 11$ km in the poleward of ±40° subset and there were only two found in the polar terrain subset. So either the central peak does not form in this suggested "mud crust" until significantly larger diameters are reached, or it does form but quickly collapses and does not leave behind an indicator it existed.

The effect is simple craters are maintained at larger diameters, but they are shallower than equatorial ones. This is more significant in high northern latitudes where there is likely a nearer surface and/or thicker cryosphere to better facilitate this. This is supported by the cohesive layered ejecta morphology distribution found in the northern hemisphere where their presence is also more prevalent than in the southern. The concentration of DLE craters in high northern latitudes supports this, for it is likely that at least this type requires a volatile in the subsurface to form based on the type's abundance over SLE on Ganymede (Boyce *et al*., 2010).

Overall, this new crater catalog with 378,540 craters $D \geq 1$ km is comparable to previous ones where they overlap, and the additional morphologies and morphometries have proven to be an unparalleled asset in studying the surface of Mars. Through this work, we have proven its utility and hope others can make use of it. Pending review, we will be making this database freely available for download via the Mars Crater Consortium section of USGS's PIGWAD server (http://webgis.wr.usgs.gov/pigwad/down/mars_crater_consortium.htm). We are also making a web-query site that allows users to download craters and features based on user-selectable fields and options that will be available at http://mars.sjrdesign.net.